MATERIALS CHEMISTRY FRONTIERS

REVIEW

View Article Online
View Journal | View Issue

Cite this: *Mater. Chem. Front.*, 2023, **7**, 4744

Near-infrared organic light-emitting materials, devices and applications

Mengxin Xu, Xinyi Li, Shihao Liu, Letian Zhang * and Wenfa Xie *

Received 22nd May 2023,
Accepted 2nd July 2023

DOI: 10.1039/d3qm00585b

rsc.li/frontiers-materials

Near-infrared (NIR) light-emitting devices have recently garnered significant interest for integration in various applications, including photodynamic therapy and component determination, with emission wavelengths ranging from 700 nm to 2500 nm. In this review, we first introduce molecular design strategies for NIR materials, with a focus on fluorescent, phosphorescent, and TADF materials, and summarize recent advancements in highly luminescent NIR materials. Secondly, we provide an overview of high-performing NIR organic light-emitting devices (OLEDs), examining their structural designs and underlying device physics. Thirdly, we highlight practical applications of NIR materials and OLEDs in areas such as biomedicine and component determination. Finally, we discuss current limitations and prospects for the development of NIR materials, devices, and applications.

1. Introduction

Near-infrared (NIR) light refers to electromagnetic radiation with a wavelength ranging from visible light to middle infrared light, typically between 700 nm and 2500 nm.[1] NIR light can easily penetrate human tissue and matches the absorption regions of certain organic molecules, making it a promising application in various fields, including biomedicine and component determination.[2–4] For instance, in photodynamic therapy, NIR luminescent materials can be utilized as photosensitizers and can effectively image tissues due to their high penetration and low autofluorescence interference.[5–8] Furthermore, due to the ability of NIR light to be absorbed by C–H, N–H, O–H, and S–H bonds in a sample, NIR spectroscopy offers notable benefits in monitoring food components. Compared to traditional methods, NIR spectroscopy is non-invasive, rapid, and requires minimal sample preparation.[9,10] As a result, research on NIR materials and light-emitting devices has become a highly sought-after topic in recent years.[11–13]

Compared to inorganic materials, organic NIR-emitting materials provide advantages on low cost, lightweight, mechanical flexibility, and biocompatibility, thus endowing them with broader potential applications and higher research value.[14–17] Organic NIR-emitting materials can be categorized into fluorescent, phosphorescent, and thermally activated delayed fluorescent (TADF) materials, each utilizing different luminescence mechanisms.[18] Radiation resulting from the transition from the lowest singlet state (S_1) and the lowest triplet state (T_1) to the ground state (S_0) is defined as fluorescence and phosphorescence respectively. TADF emitters, on the other hand, allow reverse intersystem crossing (RISC) processes at ambient temperature, leading to radiation luminescence because of the narrow energy split (ΔE_{ST}) between S_1 and T_1. Triplet excitons can transition to S_1 through RISC, and then to S_0, resulting in radiation luminescence. As both phosphorescent and TADF materials can utilize both singlet and triplet excitons, organic light-emitting devices (OLEDs) made with these materials theoretically have the potential to achieve an internal quantum efficiency (IQE) of 100%.[19,20] However, due to the small band gap of NIR materials, non-radiative decay can be significant according to the energy gap law, resulting in a photoluminescence quantum yield (PLQY) that is often below unity. Therefore, many efforts have been made to reduce the probability of non-radiative decay and greatly improve the PLQY of NIR emitters.[21,22] Currently, NIR emitter with an emission peak at 732 nm can show a PLQY over 24%.[23]

To fully harness the benefits of organic NIR emitters, the development of efficient NIR OLEDs requires precise structural design and detailed investigations into device physics. A well-designed device configuration can enhance carrier injection and transport, thereby increasing the likelihood of exciton formation.[24–27] Elaborate choice of host materials and compositional adjustment can affect the exciton distribution profile, and thus bimolecular quenching. Moreover, outcoupling efficiency (OCE) of NIR OLEDs is determined by the refractive indexes and the thicknesses of multilayer structure, light extraction units, and so on. With these efforts, the art-to-state NIR OLED have achieved a peak external quantum efficiency (EQE) of 13.4% with an emission peak at 734 nm.[28–31]

However, there are still certain limitations and challenges in NIR organic luminescent materials and devices. For NIR

State Key Laboratory of Integrated Optoelectronics, College of Electronics Science and Engineering, Jilin University, Changchun, 130012, People's Republic of China. E-mail: zlt@jlu.edu.cn, xiewf@jlu.edu.cn

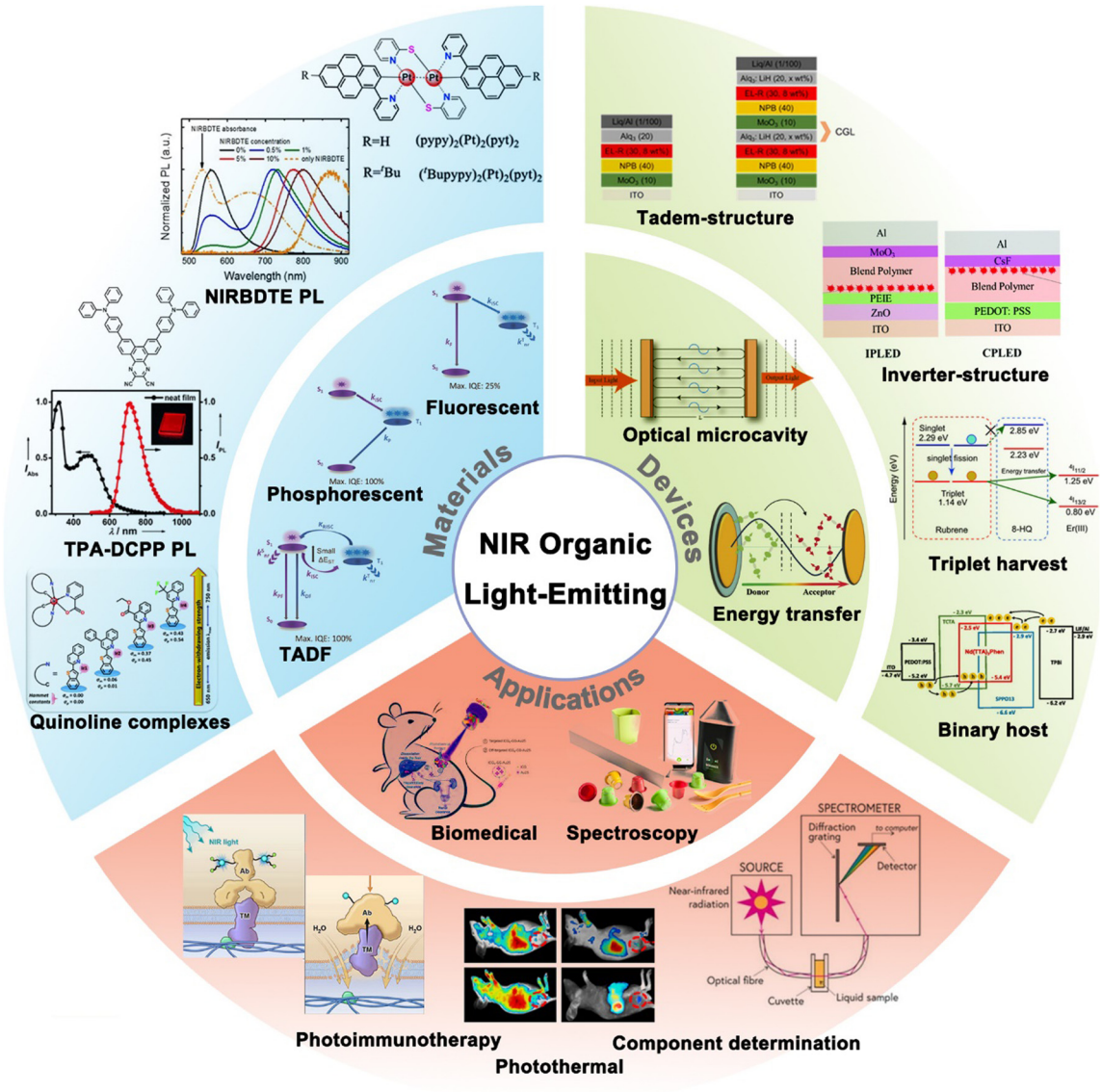

Fig. 1 General concept of NIR organic light-emitting materials, devices and applications. Reproduced with permission from ref. 26. Copyright 2020 *Journal of Materials Chemistry C*. Reproduced with permission from ref. 27. Copyright 2017 *Angewandte Chemie International Edition*.

materials, in addition to the lower PLQY, efficiency degradation or luminescence attenuation in high-temperature environments will also occur. This is because high temperatures can cause adverse effects such as structural disorder or changes in energy levels;[32] For NIR OLEDs, it is necessary to search for the optimal device structure and process parameters based on the energy level of the material; In addition, the application of NIR OLEDs usually requires integration with other devices or packaging in special environments, which will significantly increase the preparation cost of devices.[33] Therefore, research on molecular design strategies and device optimization techniques are important for further application of NIR materials and OLEDs.

Considering that current reviews have mainly focused on NIR materials, their PL properties, and their applications in photodynamic therapy or NIR spectroscopy,[34,35] this article aims to cover recent advancements in organic NIR materials, specifically their electroluminescent (EL) properties (Fig. 1). We firstly summarize the three types of EL mechanisms of NIR materials, including fluorescent, phosphorescent, and TADF materials. We then summarize advancements in the design strategies and device physics of NIR OLEDs, and examine the practical applications of NIR materials and OLEDs. Finally, we discuss the prospects of NIR materials, devices, and applications.

2. Organic near-infrared materials

2.1. Fluorescent materials

Fluorescent materials can only harvest singlet excitons, thus their maximum IQE cannot exceed 25%. Besides, the energy gap law states that the rate of non-radiative transitions in the

excited state of the semiconductor will increase exponentially with a redshift in the excitation wavelength, leading to a significantly decrease in the quantum yield.[36] As a result, the maximum EQE of NIR fluorescent OLEDs reported so far is less than 2%. Despite this, fluorescent materials have the advantages of lower cost, higher biocompatibility and great environmental friendliness compared to phosphorescent materials because they don't contain heavy metal elements. Furthermore, the exciton lifetime of fluorescent materials is 100 times shorter than that of TADF and phosphorescent materials, which provides advantages in high-speed transmission fields such as Li-Fi applications.[37] In this section, we will review the most efficient NIR fluorescent materials based on donor–accepter–donor (D–A–D) and accepter–donor–accepter (A–D–A) oligomers, polymer materials, and some unusual but promising NIR fluorescent materials.

2.1.1. D–A–D and A–D–A oligomers. In 2009, Ma and colleagues suggested that benzo(1,2-*c*:4,5-*c*′)bis((1,2,5)thiadiazole) (BBTD) could have potential advantages as a donor material in the D–A–D system due to its quinoidal character and strong electron delocalization (Fig. 2a). To prevent the weakening of chromophore aggregation, potent donor groups were added to the 4- and 8-positions of BBTD. Their demonstration of nondoped NIR OLEDs achieved an impressive EQE of 0.28% at the emission wavelength of 1080 nm.[38] In 2011, Ellinger and colleagues created a range of oligomers composed of aromatic donor units and *o*-quinoid-acceptor units (Fig. 2b). One of the oligomers, EE-BTD-EE, which had a D–A–D structure, emitted NIR light and attained EQEs of approximately 0.5%, with the EL peak appearing at 725 nm when doped into the poly(2-methoxy-5-(2-ethylhexyloxy)-1,4-phenylenevinylene) (MEH-PPV) host material.[39] In 2017, Andrea and colleagues symmetrically conjugated α,β-unfunctionalised 4,4-difluoro-4-bora-3*a*,4*a*-diaza-*s*-indacene (BODIPY) moieties with oligothienyls to create an A–D–A oligomer NIRBDTE (Fig. 2c). The BODIPY low-lying lowest unoccupied molecular orbital (LUMO) was effectively delocalized, resulting in a maximum EL emission peak at 720 nm and EQE of up to 1.1% in OLEDs.[40]

2.1.2. Polymer NIR fluorescent materials. Polymers have easily tunable emission spectra in the NIR region due to effective conjugation units and intermolecular donor–accepter (D–A) interactions.[41] In 2017, Tang and colleagues developed a series of conjugated copolymers based on indacenodithieno-3,2-*b*-thiophene (IDTT) that were with a protected alcohol group, enabling easy integration into polymer light-emitting diodes (PLEDs).[42] These copolymers demonstrated NIR emission with a peak wavelength of 705 nm and a full-width at half-maximum (FWHM) of 85 nm, yielding an impressive EQE of 0.10% in light-emitting electrochemical cells (LECs) (Fig. 3a). In 2016, Murto and colleagues developed a new set of NIR-emitting copolymers by integrating low-band-gap 6-(2-butyloctyl)-4,8-di(thiophen-2-yl)-1,2,3-triazolo4′,5′:4,5-benzo1,2-*c*-1,2,5-thiadiazole (TBTTT) segments into a high-band-gap poly 3,3′-ditetradecyl-2,2′-bithiophene-5,5′-diyl-*alt*-5-(2-ethylhexyl)-4*H*-thieno[3,4-*c*]pyrrole-4,6(5*H*)-dione-1,3-diyl (P2TTPD) host polymer backbone.[43] Efficient energy transfer was achieved by

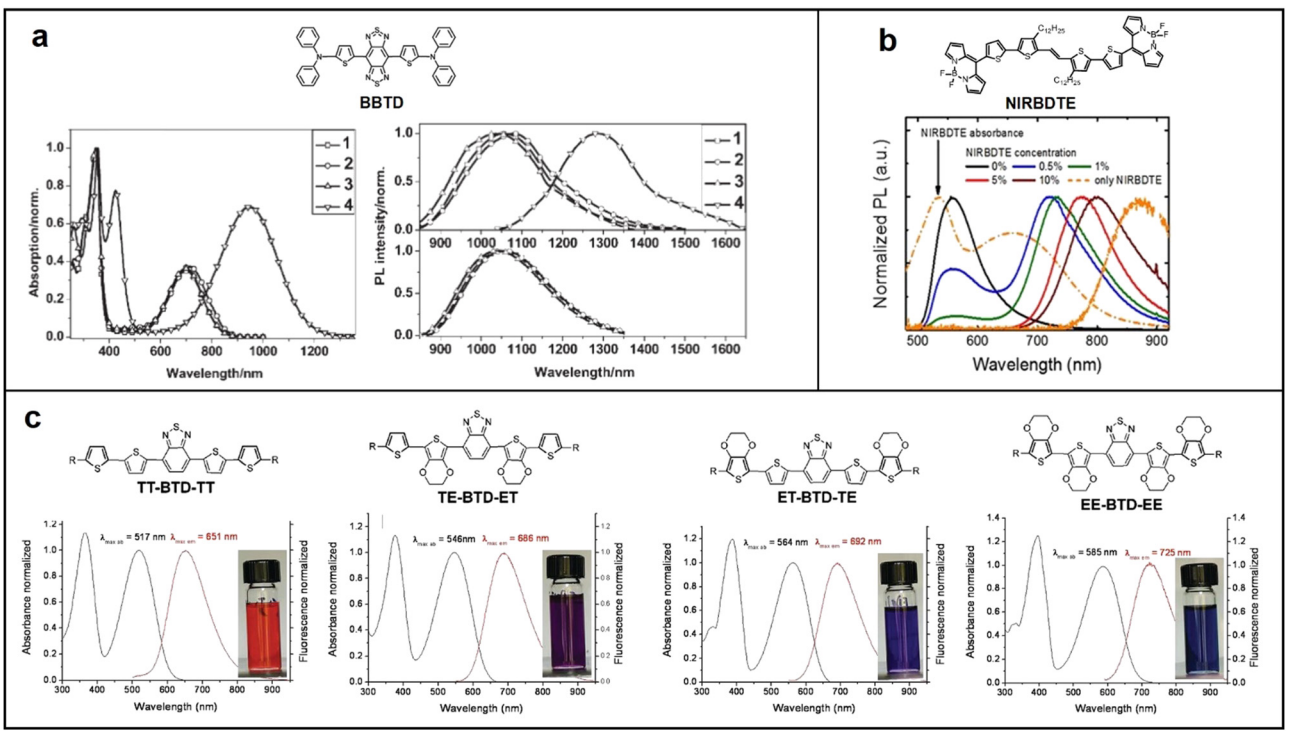

Fig. 2 Chemical structure of BBTD, absorption and emission spectra of (a) BBTD-based compounds; reproduced with permission from ref. 38. Copyright 2009 *Advanced Materials*. (b) NIRBDTE; reproduced with permission from ref. 39. Copyright 2011 *Chemistry of Materials*. (c) TT-BTD-TT, ET-BTD-TE, TE-BTD-ET, and EE-BTD-EE; reproduced with permission from ref. 40. Copyright 2017 *Scientific Reports*.

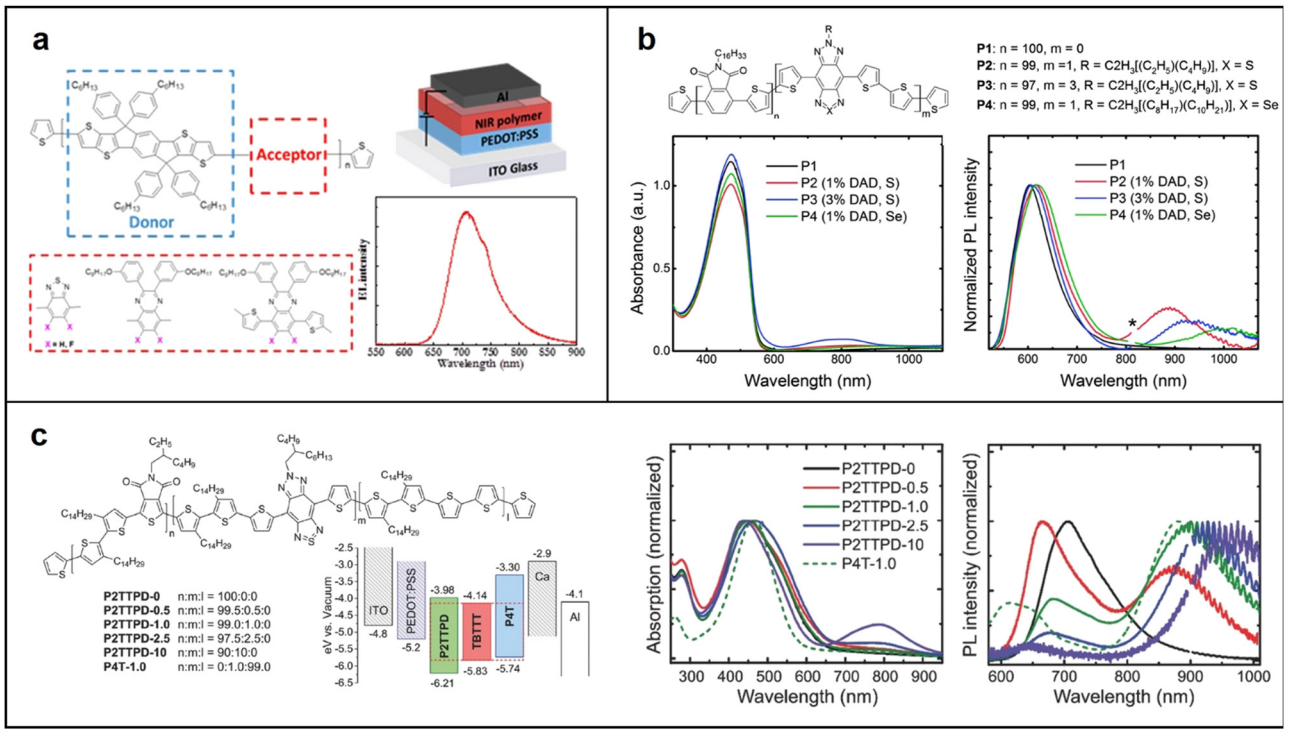

Fig. 3 (a) Chemical structure of polymer NIR emitter with IDTT as donor, and EL spectrum of PLED based on PIDTT-TQF; chemical structure, absorption and emission spectra of (b) wide-gap host polymer (P1) and the copolymers (P2, P3 and P4); Reproduced with permission from ref. 42. Copyright 2017 *Chemistry of Materials*. Reproduced with permission from ref. 43. Copyright 2016 *Advanced Optical Materials*. (c) Phthalimide–thiophene host-based copolymers. Reproduced with permission from ref. 44. Copyright 2015 *Journal of Materials Chemistry C*.

carefully controlling the intermolecular distance between the host and D–A–D segments, leading to pure NIR emission peaking at 900 nm, while keeping the V_{on} below 5 V. This study emphasized the importance of increasing the intermolecular distance between the host and D–A–D segments to enhance energy transfer efficiency and ultimately achieve higher EQE in polymer-based devices (Fig. 3b). In 2015, Giulia and colleagues made rational modifications to the chemical structure of the phthalimide-thiophene host copolymer and the NIR emitting moiety.[44] By copolymerizing with 1% D–A–D loading, the PLEDs demonstrated the highest efficiency of about 0.09% and EL peak at 895 nm. This study highlighted the effectiveness of copolymerization as a strategy to achieve nearly pure NIR EL emission (up to 95% of overall emission) for polymers based on benzothiadiazole (Fig. 3c).

2.1.3. Other NIR fluorescent material. Porphyrin derivatives are a promising fluorescent material for use as NIR emitters in OLEDs when blended with or copolymerized alongside a fluorescent host.[45] In 2011, Franco reported the red-shifted emission of linear and cyclic porphyrin hexamers in OLEDs due to their extended π-conjugation. The investigation focused on the PL and EL of these hexamers in blends with poly(9,9′-dioctylfluorene-*alt*-benzothiadiazole), where the linear hexamer showed high PL quantum efficiency of 7.7% with high color purity NIR EL luminescence (Fig. 4a).

Aggregation-induced emission (AIE) emitters have been regarded as one of the most promising materials for manufacturing high-performance OLEDs with a high EQE and low efficiency roll-off, as they emit strong light in their aggregated state and avoid the undesired ACQ effect.[46] In 2014, Wang introduced a novel approach to develop molecules with both red emission and AIE characteristics. This involved enveloping disc-shaped fluorophores with AIE fluorophores shaped like propellers, which segregated the inner large conjugated planes, thereby preventing quenching of fluorescence (Fig. 4b).[47] In 2015, Zhu conducted a synthesis of a range of new AIE-active molecules utilizing quinoline-malononitrile (QM) as the fundamental building block.[48] Variation of electron donor groups and thiophene π-bridges led to the creation of AIE-active QM derivatives exhibiting red to NIR emissions. Of these derivatives, QM-5 exhibited a considerable red shift in its emission spectra, from 668 nm in pure THF solution to 721 nm in a mixed THF/H_2O solution (Fig. 4c).

2.2. Phosphorescent materials

Typically, transitions between multiple states, such as T_1 to S_0, are forbidden due to spin prohibition. However, when the energy levels of the singlet and triplet orbitals in an organic molecule are closely spaced and located near each other, spin–orbit coupling (SOC) can occur. This phenomenon results in the display of some singlet properties by the triplet electron, leading to intersystem crossing (ISC) and phosphorescence emission. This effect is particularly notable in metal complexes containing heavy metals such as iridium (Ir), platinum (Pt),

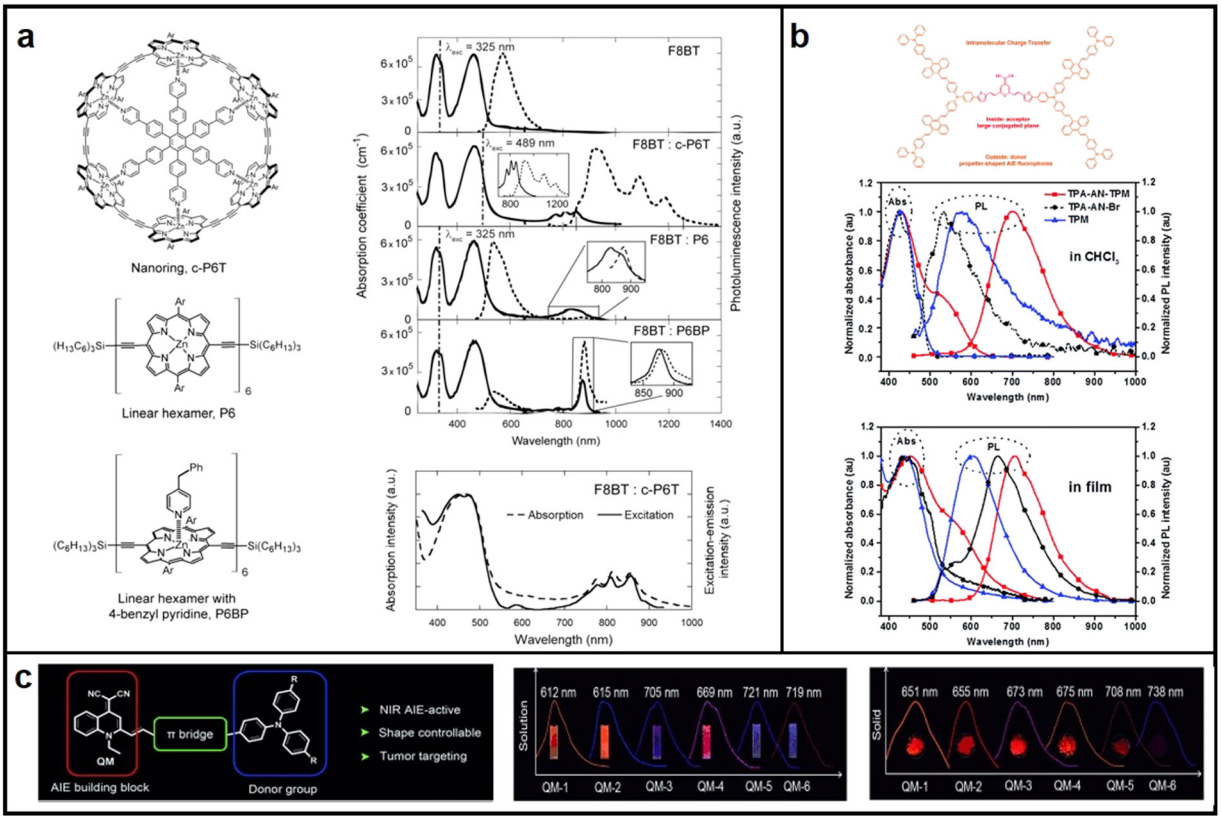

Fig. 4 Chemical structures, absorption and emission spectra of (a) porphyrin hexamers and the complex of the linear hexamer; Reproduced with permission from ref. 45. Copyright 2011 *Nano Letters*. (b) TPA-AN-TPM and TPA-AN-Br in $CHCl_3$; reproduced with permission from ref. 47. Copyright 2014 *Polymer Chemistry*. (c) QM derivative. reproduced with permission from ref. 48. Copyright 2015 *Angewandte Chemie International Edition*.

osmium (Os), palladium (Pd), europium (Eu), and terbium (Tb), *etc.* By exploiting all excitons, the IQE of materials can reach a maximum of 100%.[49–51] Therefore, phosphorescent materials have emerged as the research focus of NIR luminescent materials.

NIR-emitting phosphorescent materials are primarily classified into two groups: rare earth metal complexes and transition metal complexes. Presently, rare earth metal complexes, such as lanthanum (La), neodymium (Nd), and erbium (Er) are often inadequate for practical applications due to their low brightness.[52] In this section, we will examine recent developments in Pt and Ir NIR phosphorescent materials.

2.2.1. Platinum(II)-based materials. Platinum(II) complexes featuring a 4-coordinate square planar geometry are known to exhibit robust Pt–Pt interactions, which in turn result in unique spectral and luminescent properties, including high thermal stability and a high quantum yield.[53] These features stem from the presence of various charge transfer mechanisms, such as ligand to ligand charge transfer (LLCT), metal to ligand charge transfer (MLCT), and intramolecular ligand charge transfer (ILCT). Pt(II) complexes can be divided into two main categories: mononuclear and dinuclear/polynuclear platinum complexes.[54] Mononuclear Pt complexes are readily synthesized and exhibit higher luminous efficiency and thermal stability. In contrast, dinuclear/polynuclear Pt complexes can achieve longer-wavelength red and NIR emission by adjusting the structure of the cyclometallated ligands.[55]

Bidentate, tridentate, and tetradentate ligand complexes are the three types of mononuclear Pt complexes based on the type of ligands. Among these, bidentate ligand complexes are effective in regulating energy levels through the design of D–A structure. In 2021, Kidanu introduced AtFOND, a novel NIR material that utilized a potent donor ligand, 4-hydroxy-8-phenoxy-1,5-naphthyridine (OPhNDH), in 2-(4-methoxyphenyl)-5-(trifluoromethyl)pyridine (AtF). The introduction of OPhNDH improved the metal–metal-to-ligand charge transfer (MMLCT), leading to extremely long emission wavelengths up to maximum λ_{EL} 774 nm, but also decreased the EQE. In contrast, PBSNND, another NIR material, was created by incorporating another donor ligand, 4-hydroxy-8-dimethylamino-1,5-naphthyridine (dmaNDH), into 2-phenylbenzodthiazole (PBS), which exhibited a relatively high EQE (about 10.1%) with a maximum emission wavelength of λ_{EL} 704 nm. The high EQE was attributed to the optimal molecular arrangement of PBSNND, which increased the light OCE to 32%, a value 1.6 times higher than most conventional OLEDs (Fig. 5a).[56]

In contrast to bidentate ligand complexes, tridentate ligand complexes have potential for higher luminous efficiency due to their more rigid structures, which minimize nonradiative decay. However, ligand bond activity can lead to excimer

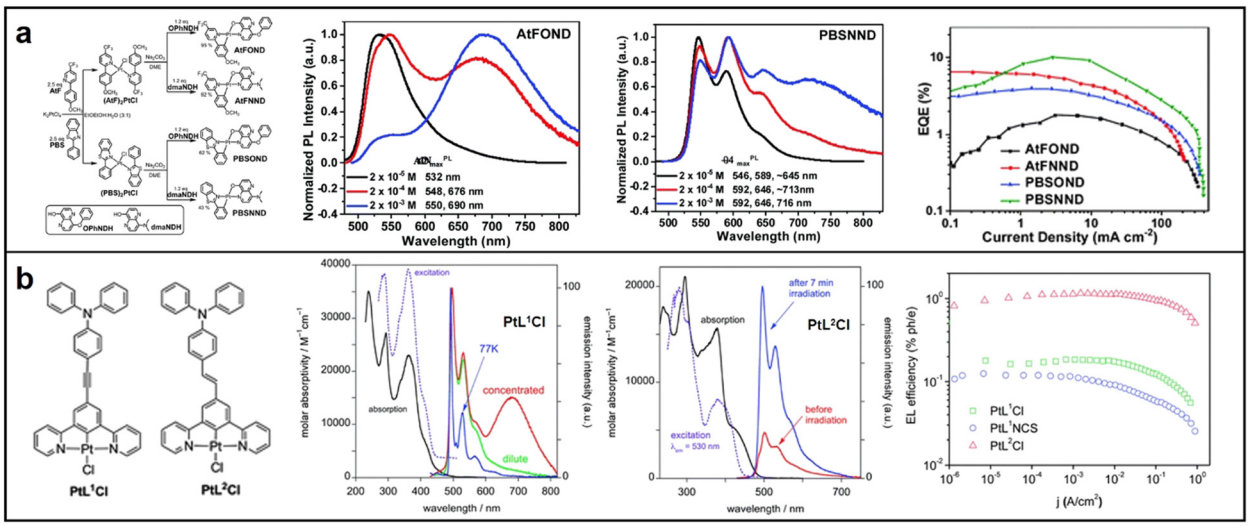

Fig. 5 Chemical structures, absorption and emission spectra, devices EQE of (a) AtFOND and PBSNND; reproduced with permission from ref. 56. Copyright 2021 *Materials Advances*. (b) PtL^{1}Cl and PtL^{2}Cl; reproduced with permission from ref. 58. Copyright 2014 *Journal of Materials Chemistry C*.

emission and greater intermolecular interactions, resulting in challenges for molecular modification and device fabrication.[57] In 2013, Filippo synthesized and characterized two highly luminous N^C^N pincer ligands and their corresponding Pt(II) complexes, PtL^{1}Cl and PtL^{2}Cl. PtL^{1}Cl is suitable for bioimaging and sensing applications owing to its high quantum yield. On the other hand, PtL^{2}Cl complexes are excellent candidates for developing NIR-OLEDs due to their high EL quantum efficiencies (Fig. 5b).[58] In 2017, Yang and colleagues reported on a group of new N^C^N-type tridentate ligands and their Pt(II) complexes with pyrimidine, which showed a unique rod-coil shape, enhanced intermolecular π–π stacking, and excellent self-assembly performance in organic solvents. Varying the concentration of the material resulted in a redshift of the maximum emission wavelength, with the emission band covering the range of 600–850 nm (Fig. 6a).[59]

Tetradentate ligand complexes are more stable than bidentate or tridentate ligand complexes due to the additional coordination sites provided by the extra donor atom. The resulting stronger metal–ligand bonds and steric hindrance provided by the arrangement of four donor atoms can prevent unwanted interactions and improve efficiency. Despite these advantages, the synthesis of tetradentate ligand complexes remains challenging, and their production can be more expensive.[60] In 2016, Huang discovered that two platinum(II) complexes, aza-triphenyltetrabenzoporphyrin (PtNTBP) and *cis*-diaza-diphenyltetrabenzoporphyrin (*cis*-PtN$_2$TBP), exhibited EL emission peaks at 848 nm and 846 nm, respectively, with maximum EQEs of 2.8% and 1.5%. These results indicated that color tuning could be achieved by replacing meso-carbon groups with nitrogen groups in a porphyrin ring, causing the EL emission peak to shift nearly 80 nm towards the infrared

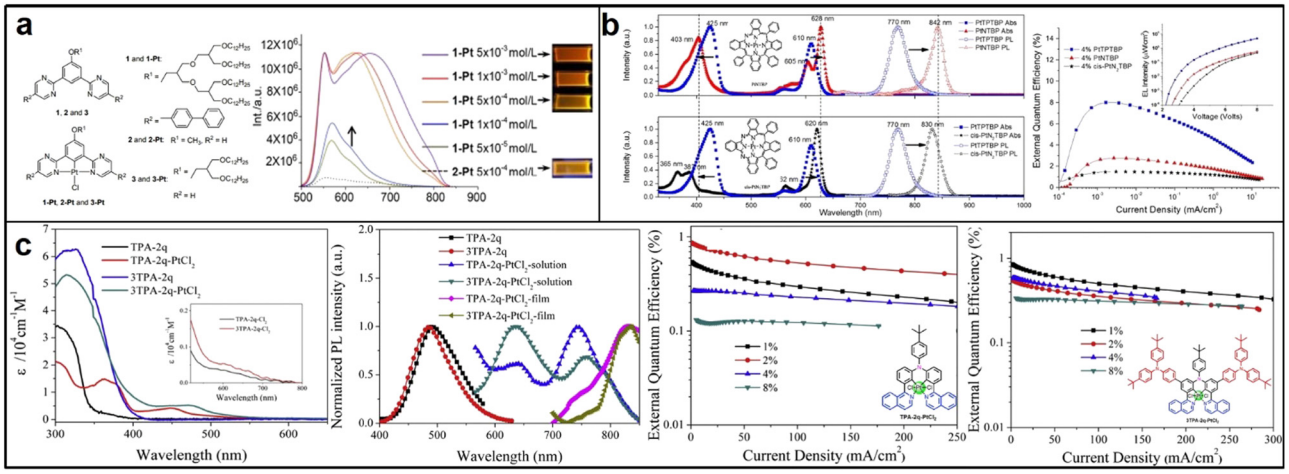

Fig. 6 (a) N^C^N-type tridentate ligand-based Pt(II) complexes; reproduced with permission from ref. 59. Copyright 2017 *Chinese Journal of Organic Chemistry* (b) PtNTBP and *cis*-PtN$_2$TBP; reproduced with permission from ref. 61. Copyright 2016 *Applied Physics Letters*. (c) TPA-2q-PtCl$_2$ and 3TPA-2q-PtCl$_2$. Reproduced with permission from ref. 62. Copyright 2017 *Dyes and Pigments*.

region, (Fig. 6b).[61] In 2017, Zhang developed two tetradentate bis-cyclometalated platinum(IV) complexes, TPA-2q-$PtCl_2$ and 3TPA-2q-$PtCl_2$, using tetradentate C^N*N^C ligands with triphenylamine units. These highly thermally stable complexes emitted EL peaks at 733 nm with an EQE of 0.87% and 750 nm with an EQE of 0.85% in their doped devices, demonstrating that tetradentate *bis*-cyclometalated platinum(IV) complexes with d^6 octahedral structures are also potential materials for PLED applications in organic NIR EL devices (Fig. 6c).[62]

Mononuclear platinum complexes have a localized excited state, resulting in emissions based on a single metal center, with a narrow absorption and emission spectrum and visible region emissions. Conversely, dinuclear or polynuclear complexes with bridging ligands enable more efficient electronic communication between metal centers. Excitation of one metal center transfers energy to neighboring metal centers, producing a delocalized excited state spread over multiple metal centers. The result is a broadened absorption and emission spectrum and NIR emissions at longer wavelengths.[63] In 2017, Su synthesized two binuclear platinum complexes, $(pypy)_2Pt_2(pyt)_2$ and $(^tBupypy)_2Pt_2(pyt)_2$, in which pypy, ^{t}Bupypy and pyt refer to 2-(1-pyrenyl)pyridine, 2-(7-*tert*-butyl-1-pyrenyl)pyridine (^{t}Bupypy) and pyridyl-2-thiolate, respectively. The unique three-dimensional chemical structure formed by the pyridyl-2-thiolate bridging units helps prevents π–π stacking and concentration quenching. Both complexes exhibited efficient NIR emission *via* metal–metal-to-ligand charge transfer (MMLCT) transition, with doped PLEDs displaying a NIR emission peak at 692 nm and a shoulder at 753 nm. The $(^tBupypy)_2Pt_2(pyt)_2$-doped devices showed the best EL performance, with a EQE_{max} of 0.74% and a maximum radiance (R_{max}) of 123.4 μW cm^{-2} at a doping concentration of 2 wt% (Fig. 7a).[64] In 2021, Marsel discovered a novel dinuclear platinum(II) complex, Pt_2(bis-dthpym)$(dpm)_2$, with a symmetric structure. This was achieved through a double N^C cyclometallation of 4,6-bis(dithienyl)-pyrimidine (H_2bis-dthpym). The coordination sphere of each Pt centre was completed by O^O-coordinating dipivaloylmethane (dpm). This structure generates low-energy unimolecular emission through twice the number of higher-lying singlet states suitable for spin–orbit coupling (SOC) with the emitting triplet state T_1, resulting in predominantly NIR emission.[65] This approach complements the increasingly popular method of exploiting bimolecular aggregates or excimers (Fig. 7b).

2.2.2. Iridium (Ir)-based materials. The synthesis of iridium-based complexes is more challenging and demanding than platinum(II) complexes for developing NIR phosphorescence materials. However, Ir-based complexes offer advantages such as increased luminous efficiency, reduced triplet–triplet annihilation (TTA) at higher currents, and shorter triplet emission lifetimes. Despite the additional complexities involved, Ir complexes are becoming a popular option in the field of NIR phosphorescence materials.[66]

A study by Qiao *et al.* in 2017 demonstrated the use of benzo[*g*]phthalazine derivatives as cyclometalated ligands to synthesize homoleptic facial NIR-emitting Ir(III) complexes tris-[1,4-di(thiophen-2-yl)benzo[*g*]phthalazine]iridium(III) ($Ir(dtbpa)_3$) and tris[1-(2,4-bis(trifluoromethyl)phenyl)-4-(thiophen-2-yl)benzo-[*g*]phthalazine]iridium(III) ($Ir(Ftbpa)_3$). These complexes exhibit NIR-emission with high PLQY of up to 5.2% at 824 nm and

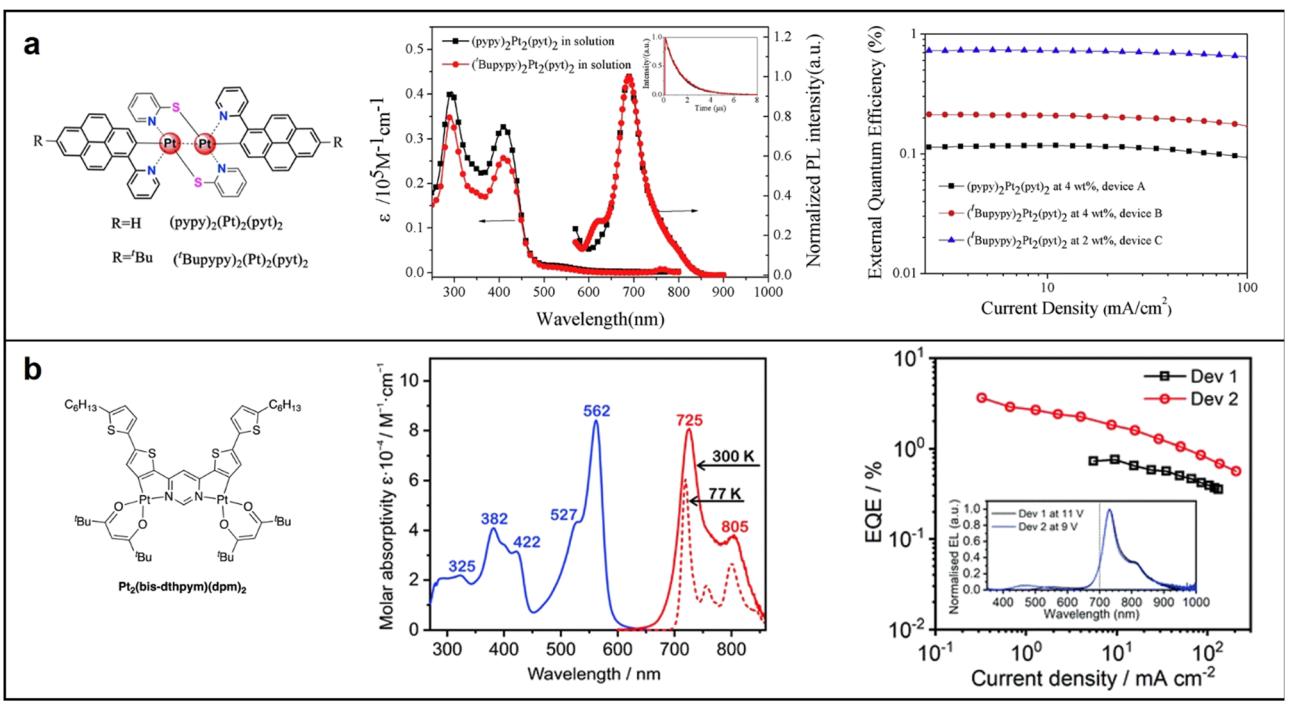

Fig. 7 Chemical structures, absorption and emission spectra, devices EQE of (a) $(pypy)_2Pt_2(pyt)_2$ and $(^tBupypy)_2Pt_2(pyt)_2$; reproduced with permission from ref. 64. Copyright 2017 *Dyes and Pigments*. (b) Pt_2(bis-dthpym)$(dpm)_2$. reproduced with permission from ref. 65. Copyright 2021 *Journal of Materials Chemistry C*.

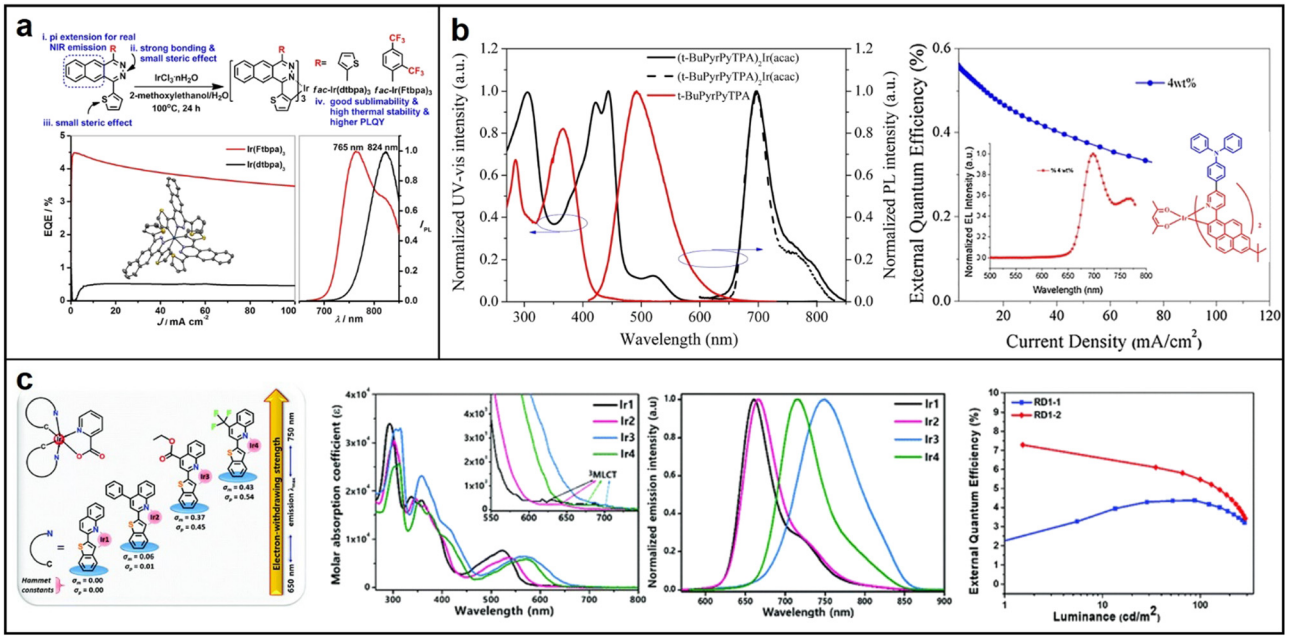

Fig. 8 Chemical structures, absorption and emission spectra, devices EQE of (a) $Ir(dtbpa)_3$ and $Ir(Ftbpa)_3$; Reproduced with permission from ref. 67. Copyright 2017 *Chemistry of Materials*. (b) (*t*-BuPyrPyTPA)2Ir(acac); reproduced with permission from ref. 68. Copyright 2018 *Chemical Physics Letters*. (c) Quinoline-based Iridium(III) complexes Ir1–Ir4. Reproduced with permission from ref. 69. Copyright 2020 *Journal of Materials Chemistry C*.

17.3% at 765 nm, respectively. It is worth mentioning that the noble metal content percentages of their complexes are around 10% Ir, which is significantly less compared to the typical green-emitting tris(2-phenylpyridine)iridium with about 30% Ir.[67] These results propose a fresh method to produce strong and long-lasting NIR emitters with high efficiency, minimal roll-off, and low cost for practical applications in NIR-OLEDs (Fig. 8a). In 2018, Liu successfully synthesized and characterized a new π-extended iridium complex $(t\text{-BuPyrPyTPA})_2Ir(acac)$ that exhibited stable NIR emission at a concentration of 4 wt%. The complex had a peak emission at 697 nm with a shoulder at 764 nm. It demonstrated a maximum EQE of 0.56% and a highest radiant emittance of 54.3 μW cm^{-2} at 119.3 mA cm^{-2}.[68] The study suggests that increasing the conjugation length of the ligand is an effective strategy to achieve stable NIR emission in PLEDs (Fig. 8b). In 2020, Kim synthesized a range of iridium(III) phosphorescent dopants by introducing substituents to the quinoline moiety of the cyclometalating ligand. The phosphorescence emission wavelength and quantum efficiencies were significantly affected by the phenyl, ethyl ester, and trifluoromethyl substituents. A high PLQY of 0.66 was recorded for Ir2 with a phenyl substituent, while Ir4 with a strong electron-withdrawing –CF3 substituent showed decent NIR emission at 716 nm with a quantum efficiency of 0.14. (Fig. 8c). Remarkably, Ir2-based OLEDs exhibited high deep-red emission with an excellent EQE of 7.29% at high doping ratios, suggesting its potential as a candidate for solution-processable PhOLEDs.[69]

2.3. TADF materials

The RISC process enables electrons in the triplet state to reach the singlet state at room temperature (298 K) when the energy of the triplet state approaches that of the singlet state. This process, along with radiation transition, allows for TADF to occur. TADF materials that undergo efficient RISC, can achieve a 100% IQE.[70–72] At present, visible emitting TADF-based OLEDs have been able to compete with phosphorescent OLEDs in terms of EQE. However, NIR TADF-based OLEDs have a low EQE, generally less than 5%, which is mainly due to the nonradiative transition process and concentration quenching effect induced by the strong D–A structure.[73] This review section will discuss recent developments in NIR TADF materials, including molecular design strategies and photophysical properties.

NIR TADF emitters typically have D–A structures, with the choice of donor and acceptor groups significantly impacting the charge transfer (CT) characteristics and photophysical properties of the emitter.[74] Commonly used electron-donating groups include pyridine, triarylamine, carbazole, and thiophene, while pyrazine derivatives, phenanthroline, benzimidazole, and tetracyanoethylene are some widely used electron-withdrawing groups.[75–77] This section will focus on NIR TADF materials that incorporate pyrazine derivatives as electron acceptors and various electron donors, as well as other NIR TADF materials that exhibit exceptional properties.

2.3.1. Pyrazine derivatives based NIR TADF materials. In 2015, Wang *et al.* reported the synthesis of TPA-DCPP, possessing a D–π–A–π–D structure, with triphenylamine (TPA) as the donor and 2,3-dicyanopyrazino phenanthrene (DCPP) as the acceptor. The molecule achieved a small ΔE_{ST} value of 0.13 eV and a large fluorescence rate (k_F) value of 9.0×10^{-7} s^{-1}. Furthermore, TPA-DCPP exhibited a high Φ_{PL} value of 14% with an emission at λ = 708 nm in the neat film. Using TPA-DCPP as a

nondoped emitter, the researchers fabricated an OLED that demonstrated a maximum EQE of 2.1% with CIE coordinates of (0.70, 0.29).[78] Interestingly, when TPA-DCPP was used as a doped emitter, the device exhibited an extraordinarily high EQE of 9.8% with an emission at λ = 668 nm, which is comparable to the most efficient deep-red/NIR PHOLEDs with similar EL spectra (Fig. 9a). This study introduces a novel approach to designing efficient organic NIR fluorescent molecules, which has significant implications for the development of next-generation NIR OLEDs. In 2020, Yu *et al.* reported on the utilization of anthryleno-1,2-bpyrazine-2,3-dicarbonitrile (DCPA) derivatives as NIR-emitting materials. Two emitters, namely DCPA-TPA and DCPA-BBPA, were designed and synthesized by functionalization with aromatic amine donors. The strong intramolecular charge transfer interactions between the amine donors and the DCPA acceptor led to the generation of large dipole moments, and the extended π skeleton on the acceptor segments can effectively enhance the electron-withdrawing ability of DCPA. The emission of the neat films of DCPA-TPA and DCPA-BBPA can be fully extended into the NIR region (>700 nm) with increasing doping ratio (Fig. 9b). Additionally, non-doped devices based on DCPA-TPA and DCPA-BBPA emit in the NIR region with peaks at 838 and 916 nm, and a maximum radiance of 20 707 mW Sr^{-1} m^{-2} was achieved.[79] This work presents a simple and efficient molecular design strategy for developing NIR-emitting materials. In 2021, Balijapalli conducted a study introducing a new electron donor D–A TADF molecule, 11,12-bis(4-(diphenylamino)phenyl)dibenzo[*a*,*c*]phenazine-2,3,6,7-tetracarbonitrile (TPA-PZTCN), which displays strong NIR EL luminescence (EQE_{max}: 13.4% ±0.8%) at 734 nm with excellent EQE roll-off suppression (EQE > 10% at 1 mA cm^{-2}). The efficient TADF can be attributed to the rigid and strong electron-withdrawing core of PZTCN, which facilitates the harvesting of triplets and sensitizing of deeper-NIR-fluorophores. Furthermore, the TADF-sensitized NIR-OLED utilizing TPA-PZTCN demonstrates excellent device durability, with a lifetime exceeding 600 hours at an LT_{95} threshold (Fig. 10a).[80] In 2022, Wang reported the discovery of a novel NIR TADF molecule named CNPP-TPA. This molecule contains triphenylamine (TPA) as the donor and 2,3-dicyanopyrazino phenanthroline (CNPP) as the acceptor. The strong electron-withdrawing ability and the intramolecular hydrogen bond present in CNPP-TPA result in NIR photoluminescence with a peak at 701 nm, with a PLQY of 96.5% (Fig. 10b). This is attributed to the rapid singlet radiation and effective RISC. Furthermore, the doped film of CNPP-TPA possesses a rigid structure, with a balanced enhancement of intermolecular charge transfer and quenching suppression, leading to a PLQY of 96.5% and a near-zero ΔE_{ST} of 0.08 eV.[81] In 2022, Fan' group developed a novel D–A1–A2–A3 configuration NIR TADF material named TPA-CN-N4-2PY. This material incorporated three distinct sub-acceptor units, cyano (CN), dipyrido-3,2-*a*:2′,3′-*c*-phenazine (N4), and pyridine (PY), into the chemical structure to enhance its electron-accepting capability. By introducing two pyridine units to TPA-CN-N4, the resulting TPA-CN-N4-2PY had an extended π-backbone, which shifted the EL emission to the NIR region and simultaneously improved the horizontal ratio of emitting dipole orientation. When applied in OLEDs, TPA-CN-N4-2PY achieved a record-breaking EQE of 21.9% with an emission peak at 712 nm at a doping ratio of 9.0 wt%. This approach of utilizing multiple sub-acceptors could offer a new direction for creating NIR-TADF materials (Fig. 10c).[82]

2.3.2. Other NIR TADF materials. In 2018, Ye and colleagues conducted a study aimed at prolonging the NIR TADF and amplified spontaneous emission (ASE) while preserving efficiency by modifying the chemical structure. They successfully synthesized a novel dimeric borondifluoride curcuminoid

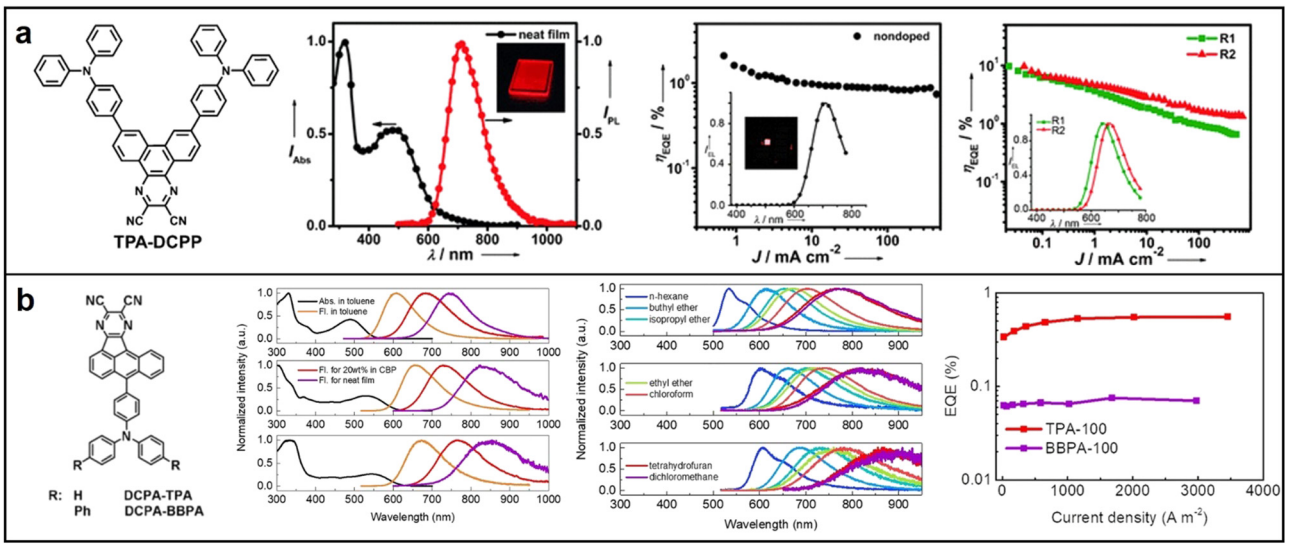

Fig. 9 Chemical structures, absorption and emission spectra, devices EQE of (a) TPA-DCPP; Reproduced with permission from ref. 78. Copyright 2015 *Angewandte Chemie International Edition*. (b) DCPA-TPA and DCPA-BBPA; Reproduced with permission from ref. 79. Copyright 2020 *Angewandte Chemie International Edition*.

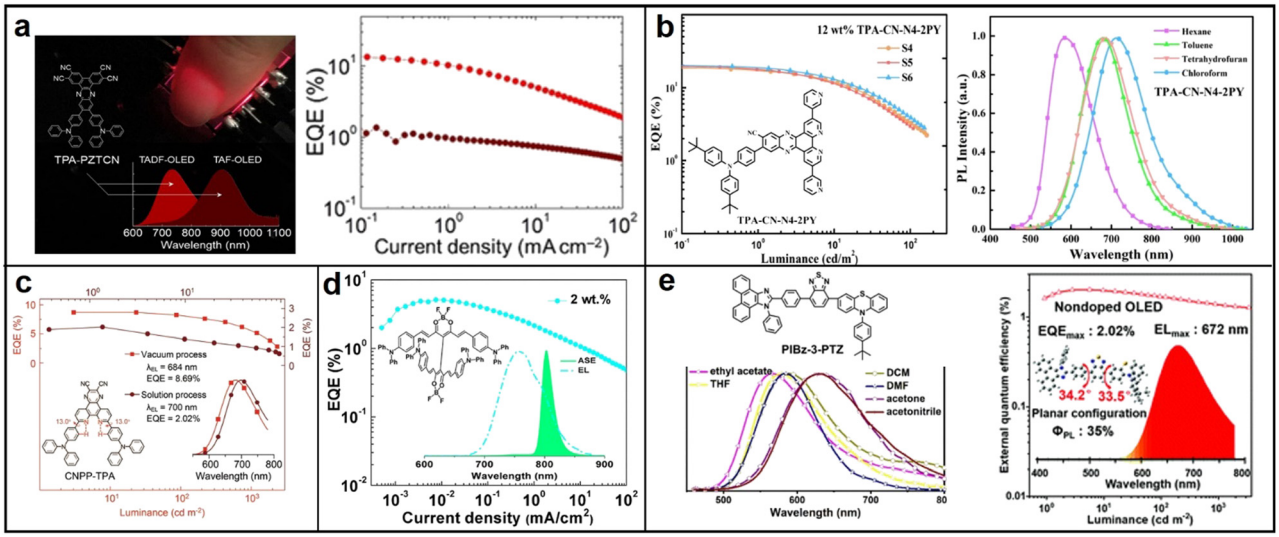

Fig. 10 (a) TPA-PZTCN; reproduced with permission from ref. 80. Copyright 2021 *Angewandte Chemie International Edition*. (b) CNPP-TPA; reproduced with permission from ref. 81. Copyright 2022 *Chemical Engineering Journal*. (c) TPA-CN-N4-2PY; reproduced with permission from ref. 82. Copyright 2022 *Materials Horizons*. (d) TADF-ASE emitter; reproduced with permission from ref. 83. Copyright 2018 *Chemistry of Materials*. (e) PIBz-3-PTZ. Reproduced with permission from ref. 84. Copyright 2020 *Journal of Materials Chemistry C*.

derivative (4,4′,4″,4‴-((1*E*,1′*E*,1″*E*,1‴*E*)-(2,2,2′,2′-tetrafluoro-2*H*,2′*H*-1λ^3,1′λ^3,2λ^4,2′λ^4-[5,5′-bi(1,3, 2-dioxaborinine)]-4,4′,6,6′-tetrayl)tetrakis(ethene-2,1-diyl))tetrakis (*N*,*N*-diphenylaniline)), that is easily processed in solution and possesses exceptional photophysical, EL and ASE properties. The study's most effective OLED produced a peak emission wavelength of 758 nm and achieved a maximum EQE of 5.1% (Fig. 10d).[83] In 2020, Liu reported on the synthesis of three novel D–A–D fluorophores named PIBz-10-PTZ, PIBz-10P-PTZ, and PIBz-3-PTZ, utilizing phenanthro-9,10-dimidazole and phenothiazine as donors and benzothiadiazole as the acceptor. Due to the unilateral steric hindrance between adjacent hydrogen atoms along the horizontal axis, PIBz-3-PTZ demonstrated a fully conjugated structure and completely planar conformation. PIBz-3-PTZ also exhibited strong dual resonance (DR) emission and AIE properties, with a high PLQY of 35% in neat thin films. The non-doped OLEDs incorporating PIBz-3-PTZ displayed a maximum EQE of 2.02% at an emission peak of 672 nm (Fig. 10e).[84]

The NIR luminescent materials and their properties mentioned above are summarized in Table 1.

3. Near-infrared organic light-emitting devices

Since its inception by Tang and VanSlyke in 1987,[85] OLED technology has made remarkable progress. Today, OLED has become one of the most popular display technologies due to its ultrathin, lightweight, flexible, foldable, and biocompatible properties.[86–88] These features make OLEDs ideal for applications in fields such as NIR biomedicine, NIR spectroscopy, and others. In this section, the mechanism and luminescent characterization of OLEDs will be introduced first, followed by a review of recent research on high-efficiency NIR OLEDs, with an emphasis on device structure design and physics.

3.1. Operating mechanism and luminescent characterization

The light-emission process in OLEDs follows a sequence of four steps. Initially, electrons and holes are injected into the organic layers between the cathode and anode, respectively. Secondly, the carriers are transported towards the emitting layer (EML) under the influence of an electric field. Thirdly, the combination of electrons and holes results in the formation of excitons. Finally, radiation transitions occur as the excitons return to the ground state, resulting in light emission.[89] Each of the processes mentioned above has a significant impact on the luminescent properties of the device. The quality of OLEDs is usually evaluated by the luminous efficiency (LE), which is a measure of the combined effects of the above processes. There are three ways to express LE. The first is known as current efficiency (CE), which represents the percentage of the device's emission brightness to the injection current density and is expressed in cd A^{-1}. The second is power efficiency, which represents the percentage of output optical power to input power and is expressed in lm W^{-1}. The third is quantum efficiency, which represents the percentage of the device's emission brightness to injection current density and is expressed as a percentage.[90,91] Notably, there are two types of quantum efficiency: IQE and EQE. IQE represents the percentage of the total number of photons generated by the device as a percentage of injected carriers, while EQE represents the percentage of photons emitted from the device as a percentage of injected carriers. EQE is the most commonly used efficiency term as it is independent of the photopic weighting factor and takes into account all

Table 1 NIR organic luminescent materials

Class		Material	$\lambda_{max,PL}$ (nm)	Φ_{PL} (%)	$\lambda_{max,EL}$ (nm)	EQE_{max} (%)	Ref.
Fluorescent material	D–A–D oligomer	BBTD	1255	0.5	1080	0.28	38
		EE-BTD-EE	725	0.07	—	0.87	39
	A–D–A oligomer	BODIPY derivative	—	20	720	1.1	40
	Polymer	IDTT	—	19	705	0.1	42
		P2TTPD	924	—	909	0.01	43
		Phthalimide–thiophene polymer	890	31	895	0.09	44
	Porphyrin derivative	c-P6T	920	7.7	960	0.024	45
	AIE emitter	TPA-AN-Br	706	12.9	—	—	47
		QM	721	—	—	—	48
Phosphorescent material	Platinum(II)	PBSNND	732	33	704	10.1	56
		PtL^2Cl	702	0.003	685	1.2	58
		N^C^N-type complex	685	—	—	—	59
		PtNTBP	842	—	848	2.8	61
		cis-PtN_2TBP	830	—	846	1.5	61
		TPA-2q-$PtCl_2$	742	—	733	0.87	62
		3TPA-2q-$PtCl_2$	758	—	750	0.85	62
		$(pypy)_2Pt_2(pyt)_2$	690	2.89	692	0.22	64
		$(^tBupypy)_2Pt_2(pyt)_2$	690	6.80	692	0.74	64
		$Pt_2(bis\text{-}dthpym)(dpm)_2$	725	0.17	731	3.6	65
	Iridium(III)	$Ir(dtbpa)_3$	824	5.2	811	0.5	67
		$Ir(Ftbpa)_3$	765	17.3	760	4.5	67
		$(t\text{-}BuPyrPyTPA)_2Ir(acac)$	697	1.92	697	0.56	68
		Ir4	716	0.12	716	1.07	69
TADF material	Pyrazine derivative	TPA-DCPP	708	14	710	2.1	78
		DCPA-TPA	824	75	838	0.58	79
		DCPA-BBPA	854	73	916	0.07	79
		TPA-PZTCN	729	19.1	734	13.4	80
		CNPP-TPA	701	96.5	700	2.02	81
		TPA-CN-N4-2PY	653	68	712	21.9	82
	Others	Borondifluoride derivative	760	45	758	5.1	83
		PIBz-3-PTZ	643	58	672	2.02	84

observation directions. They can be expressed as follows:[92]

$$IQE = \eta_r \chi \frac{K_r}{K_r + K_{nr}} \quad (1)$$

$$EQE = \eta_e IQE \quad (2)$$

In the equation, η_r is the ratio of the number of recombined carriers to the number of injected carriers, χ is the ratio of excitons used to generate light emission to the total number of excitons, K_r and K_{nr} represent the rates of the optical and non-optical radiation processes generated by the excited state, respectively, and η_e is the OCE.

At present, OLEDs based on high-efficiency phosphorescent and TADF materials can achieve almost 100% IQE, while the EQE is generally less than 30%.[92] This is primarily because the energy generated by the dipole emitter is transferred to various modes, causing significant energy loss. To address this issue, we will use the normalized in-plane wavevector (u) to analyze the light propagation and coupling in OLEDs, as it is conserved across all boundaries and dielectric media. It is expressed as follows:[93]

$$u = \frac{k_{||}}{\left|\vec{k}\right|} = \sin\theta \quad (3)$$

where $\vec{k}$ is the wavevector, $k_{||}$ is the horizontal component of $\vec{k}$, and θ is the angle between the direction of light propagation and the normal direction. As θ changes, light displays four distinct modes: the air mode, substrate mode, waveguide mode, and surface plasmon polariton (SPP) mode. The air mode refers to the portion of light transmitted outside the OLED, and the proportion of this mode to the total is the OCE. The substrate mode refers to the portion of light confined within the substrate due to total internal reflection (TIR) at the interface between the substrate and air. The waveguide mode indicates the portion of light confined within the optical cavity of an OLED due to TIR at the electrode surface. The SPP mode refers to the electromagnetic waves generated by the coupling of photons and metal surface plasmons. Table 2 illustrates the relationship between the value of θ and the different modes. The OCE of an OLED with an optimized structure is typically between 20–30%, resulting in a relatively low EQE value.[94] Currently, strategies to improve the EQE of NIR OLEDs are centered on two aspects: optical microcavity design and exciton energy transfer optimization.[95–101]

3.2. High efficiency NIR OLEDs

3.2.1. Optical microcavity design. In OLEDs, the optical microcavity is composed of two conductive plane mirrors and

Table 2 Relationship between the value of θ and the different modes

Channels	Modes	θ (rad)
Outcoupling	Air mode	$0 < \theta < \theta_{c_1} = \sin^{-1}(1/n_{org})$
	Substrate mode	$\theta_{c_1} < \theta < \theta_{c_2} = \sin^{-1}(n_{sub}/n_{org})$
Loss	Waveguide mode	$\theta_{c_2} < \theta < \pi/2$
	SPP mode	Undefined

behaves similarly to a Fabry–Perot resonant cavity. According that the emission intensity $I(\lambda,\theta)$ of microcavity devices is related to the emission wavelength λ and emission angle θ, which can be calculated using eqn (4):

$$I(\lambda,\theta)=\frac{T_t\left[1+R_b+2\sqrt{R_b}\cos\left(-\Phi_b+\frac{4\pi nz\cos(\theta_{org,EML})}{\lambda}\right)\right]}{\left(1-\sqrt{R_tR_b}\right)^2+4\sqrt{R_tR_b}\sin^2\frac{\Delta\Phi}{2}}I_0\lambda \quad (4)$$

where T and R are the transmittance and reflectivity of the electrode, Φ_b is the phase shift of the bottom electrode, and z is the distance from the luminescent material to the reflecting electrode. The factor I_0 is the emission intensity of radiating molecules. After one cycle of the light wave, the phase shift $\Delta\Phi$ given by eqn (5):

$$\Delta\phi=-\phi_b-\phi_t+\sum_i\frac{4\pi n_id_i\cos(\theta_{org,i})}{\lambda} \quad (5)$$

where m is the mode index, d_i is the microcavity length, and n_i is the refractive index of all organic layers in the cavity.[102] This structure is characterized by the resonance condition, whereby the incident light's wavelength causes an enhancement of the transmitted light intensity, resulting in a sharp peak in the transmission spectrum. Conversely, other wavelengths experience destructive interference. This phenomenon is known as the microcavity effect.[95] According to the resonance condition of microcavities, an increase in microcavity length results in a corresponding increase in the resonance wavelength. Despite this relationship, the issue of low NIR PL intensity has persisted. In 2022, Park presented a solution to this problem by demonstrating that tandem-structured microcavity devices are capable of producing stronger NIR emission than single devices with increased cavity length. The fabrication process entailed utilizing a red emitter, tris(1-phenylisoquinoline)iridium(III) ($Ir(piq)_3$), which possesses a broad PL peak spanning 550 to 800 nm. The tandem device ultimately achieved superior performance characterized by a narrow FWHM of 34 nm, high radiant emittance exceeding 5 mW cm^{-2}, and EQE of 19.17% (Fig. 11a). This outcome was attributed to the combination of a sophisticated microcavity structure with an efficient charge generation layer.[96] In 2021, Wong investigated the effect of optical characteristics on the EQE of NIR OLEDs by precisely designing the energy levels of materials and utilizing the optical simulation software Setfos. The devices consisted of four different electron transport layer (ETL) thicknesses (30, 50, 100, and 150 nm). The simulation results have revealed a direct correlation between the EQE and OCE for varying ETL

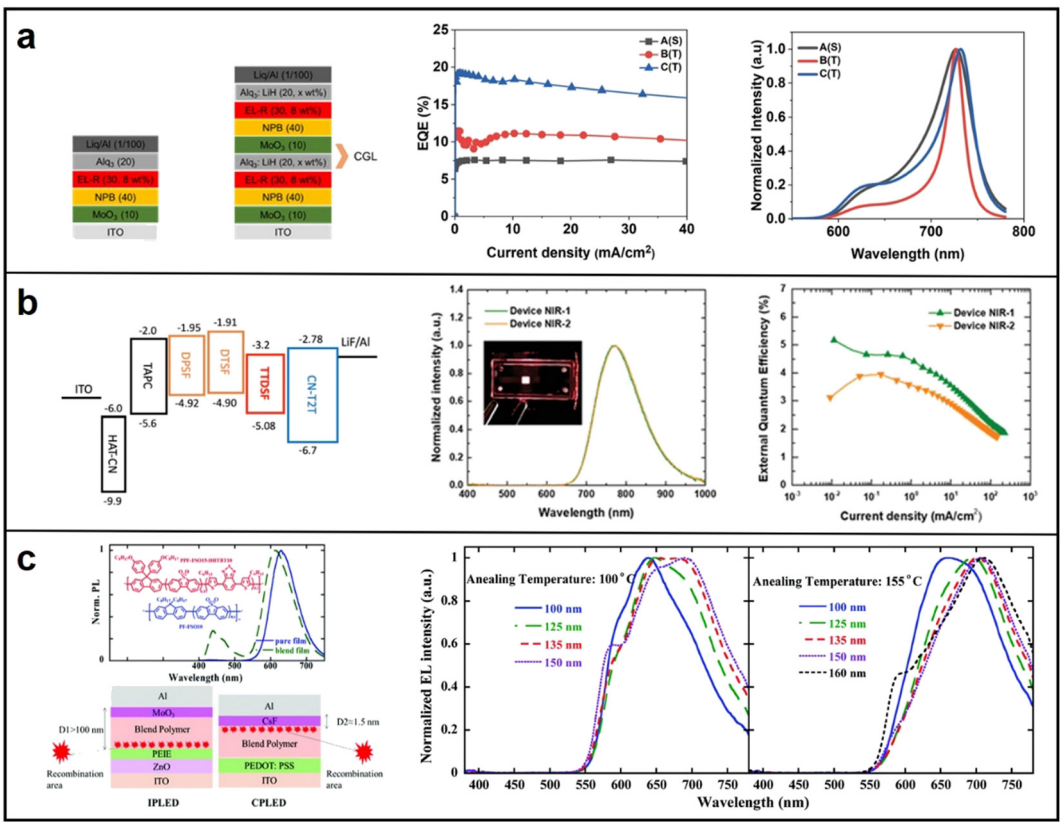

Fig. 11 (a) Device structure of single and tandem OLEDs, EQE of single OLED, tandem OLEDs with Ag (20 nm) and Ag(30 nm), respectivity. Reproduced with permission from ref. 96. Copyright 2022 *Scientific Reports*. (b) Energy levels, EL Spectra and EQE of DPSF:CN-T2T and DPSF:CN-T2T:TTDSF-based OLEDs, respectivity. Reproduced with permission from ref. 97. Copyright 2021 *Advanced Optical Materials*. (c) Device Structure and EQE of inverted microcavity devices. Reproduced with permission from ref. 98. Copyright 2019 *Journal of Materials Chemistry C*.

thicknesses. In addition to the intrinsic PL of the emitter, the OLEDs caused a further red-shift of the EL_{max} wavelength, resulting in a peak emission at 774 nm and an EQE of up to 5.3% (Fig. 11b).[97] In 2019, Xu accomplished the generation of NIR emissions from traditional red fluorescent polymers by investigating the relationship between the exciton recombination region and the thickness of the EML in inverted structures. By incorporating the microcavity effect to fine-tune the emission spectrum of the device and precisely manipulating the thickness of the emissive layer, inverted devices based on PPF-FSO15-DHTBT10 and MEH-PPV were successfully fabricated. These devices emitted NIR light at 700 nm and 706 nm, respectively, and exhibited a EQE_{max} of 0.54% and 1.03% (Fig. 11c). These findings are of significant importance for the advancement of high-efficiency NIR OLEDs and related structural designs.[98]

3.2.2. Exciton energy transfer optimization. In the condensed phase, polyatomic molecules with emission energy gaps in the NIR region will exhibit significantly reduced emission intensities. The mechanism responsible for suppressing NIR emission is widely acknowledged as the energy gap law. According to this law, unless there is a crossing between two potential energy surfaces, the relaxation process from the S_1 or T_1 state to the S_0 state can be facilitated by the overlap of wavefunctions between the lowest vibrational level of S_1 or T_1 and the higher isoenergetic vibrational levels of the S_0 state. This is followed by rapid vibrational relaxation to the lowest vibrational level of the S_0 state through the release of heat. The rate of vibrational relaxation increases as the emission gap shifts towards the deep red and NIR regions,[103] leading to low exciton utilization. It is believed that facilitating energy transfer through structural design of OLEDs is an effective method for enhancing exciton utilization. In 2018, Ryo and colleagues demonstrated that triplets generated through singlet fission in a rubrene host matrix emit NIR EL by erbium(III) tris(8-hydroxyquinoline) (ErQ_3) after excitonic energy transfer from the "dark" triplet state of rubrene to an "emissive" state of ErQ_3. Consequently, the overall exciton production efficiency reached 100.8%, exceeding the 100% theoretical limit.[99] This finding also implies that achieving 200% efficiency is possible by converting all electrically generated excitons to singlets (Fig. 12a). In 2017, Adachi presented an effective NIR TADF-sensitized OLED that utilized (triphenylamine-2,3-dicyanopyrazino phenanthrene) (TPA-DCPP) as a TADF sensitizer and the 4,9-bis4-(*N*,*N*-diphenylamino)phenyl-6,7-diphenyl1,2,5thiadiazolo3,4-gquinoxaline (TPA-ThQ) NIR fluorophore. TADF-sensitized fluorescence involved the rapid transfer of thermally upconverted singlet excitons from the TADF host to a fluorescent guest *via* Förster resonance energy, thereby achieving high luminous efficiency and suppressing efficiency roll-off. The optimized devices in experiments exhibited an EQE of 3.8% at a wavelength of 780 nm

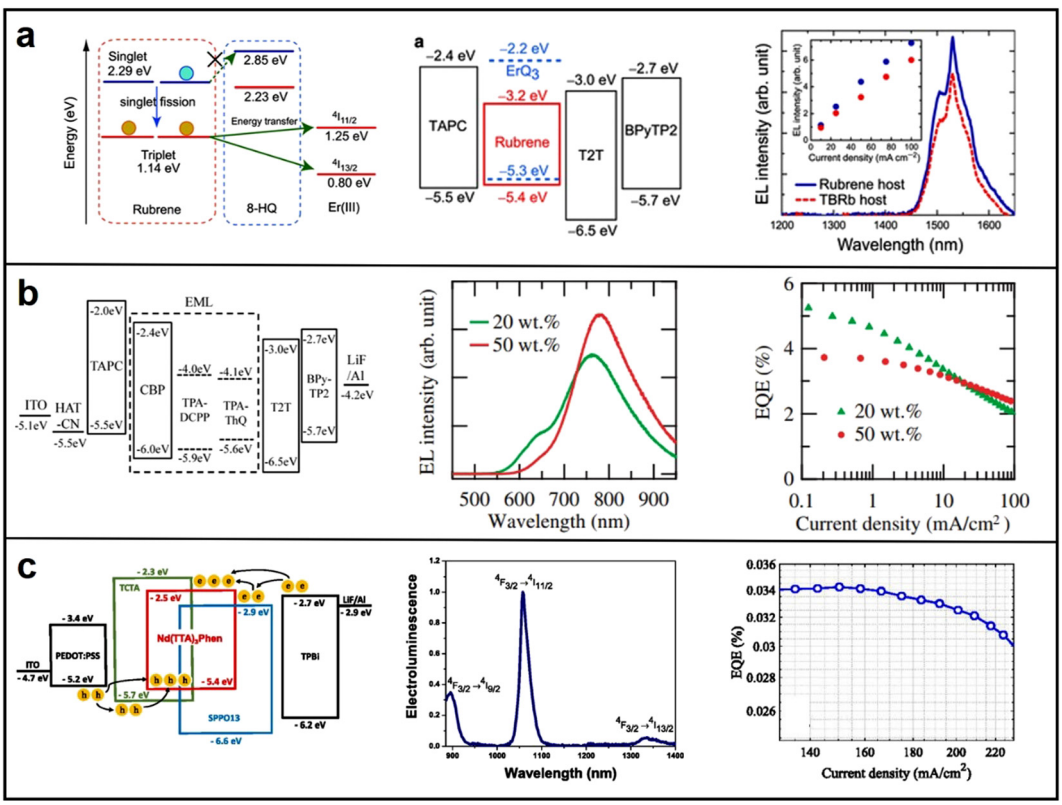

Fig. 12 (a) Jablonski diagram for the harvesting of triplets of ErQ_3 (left), energy level (middle) and EL spectrum (right) of OLEDs with a host of rubrene or TBRb; energy level, EL spectrum and EQE of (b) TADF-sensitized OLEDs and (c) $Nd3^+$ ions-based binary ambipolar host OLEDs. Reproduced with permission from ref. 99. Copyright 2018 *Advanced Materials*. Reproduced with permission from ref. 100. Copyright 2008 *Applied Physics Express*. Reproduced with permission from ref. 101. Copyright 2019 *Applied Physics Letters*.

Table 3 High efficiency NIR OLEDs

Optimization strategy	Emitter	Host	Device structure	$\lambda_{max,EL}$ (nm)	EQE_{max} (%)	Ref.
Optical microcavity design	$Ir(piq)_3$	$Bebq_2$	ITO/MoO_3 (10 nm)/NPB (40 nm)/$Bebq_2$:$Ir(piq)_3$ (30 nm, 8 wt %)/Alq_3:-LiH (20 nm, 5 wt%)/MoO_3 (10 nm)/NPB (40 nm)/$Bebq_2$:$Ir(piq)_3$ (30 nm, 8 wt%)/Alq_3:LiH (20 nm, 2 wt%)/Liq (1 nm)/Al (100 nm)	730	19.17	96
	DTSF	CN-T2T	ITO/HAT-CN (30 nm)/TAPC (70 nm)/DTSF (15 nm)/DTSF:CN-T2T (50 wt%, 30 nm)/CN-T2T (50 nm)/LiF (1 nm)/Al (100 nm)	746	5.3	97
	PPF-FSO15-DHTBT10	PF-FSO10	ITO/ZnO/PEIE/PF-FSO10:PPF-FSO15-DHTBT10/MoO_3 (10 nm)/Al (120 nm) (No thickness provided)	700	0.54	98
Exciton energy transfer optimization	ErQ_3	Rubrene	ITO/TAPC (50 nm)/2 wt% ErQ_3:rubrene (30 nm)/T2T (10 nm)/BPy-TP2 (55 nm)/LiQ (2 nm)/Mg:Ag (15 nm)	1530	—	99
	TPA-ThQ	CBP	ITO (100 nm)/HAT-CN (10 nm)/TAPC(50 nm)/CBP, 5 wt% TPA-DCPP (30 nm)/T2T (20 nm)/Bpy-TP2 (60 nm)/LiF (0.8 nm)/Al (100 nm)	780	3.8	100
	$Nd(TTA)_3Phen$	SPPO13 and TCTA	ITO/PEDOT:PSS (35 nm)/SPPO13 : TCTA : $Nd(TTA)_3Phen$ (6 : 3 : 1) (20 nm)/TPBi (40 nm)/LiF (0.8 nm)/Al (100 nm)	890	0.034	101

(Fig. 12b).[100] In 2019, Adachi integrated a Nd^{3+} complex consisting of thenoyltrifluoroacetone and 1,10-phenanthroline ligands into a co-host system that facilitates exciplex formation. This unique binary ambipolar host system promotes direct charge trapping and exciton formation on the Nd^{3+} complex molecules, resulting in efficient energy transfer from the singlet and triplet exciplexes generated between the host molecules to the Nd^{3+} ions, thereby enhancing luminescence efficiency. The PLQY of this blend is 1.2%, and the optimized OLED achieves a maximum EQE of 0.034% (Fig. 12c).[101]

The NIR OLEDs and their properties mentioned above are summarized in Table 3.

4. Application areas of NIR materials and OLEDs

4.1. Photothermal and photoimmunotherapy

4.1.1. Photodynamic therapy. Photodynamic therapy (PDT) is a medical technique that utilizes a light source and a photosensitizing agent to eradicate abnormal cells or tissues. The light source can use flexible NIR OLED with high optical power to achieve adhesion with the skin and reduce the loss of optical power,[96] while the photosensitizing agent can be administered through either injection or topical application to the targeted area where it is absorbed by the affected cells or tissues (Fig. 13a).[104,105] Upon absorption, the agent is activated by a specific wavelength of light, inducing the generation of reactive oxygen species that can lead to the destruction or impairment of the targeted cells. PDT is commonly used as an alternative treatment for several medical conditions, including various cancers, skin disorders, and eye diseases, as it is less invasive and has fewer adverse effects than traditional treatments such as chemotherapy.[106,107]

To ensure optimal efficacy in therapy and imaging, photosensitizing agents must exhibit certain key properties, such as high absorption at the treatment wavelength, safety in the absence of light, stability during the treatment process, favorable biocompatibility, and efficient accumulation in the targeted tissue.[108] These agents can be broadly classified into several categories, including organic molecules, nanoparticles, carbon-based materials, and other inorganic materials. Our discussion will mainly focus on the potential application of NIR organic molecules and their corresponding nanoparticles.[109] In 2016, Yu and colleagues prepared nanoparticles FA-RSV/ICG-PLGA-lipid NPs (FA-RIPNPs) by encapsulating indocyanine green (ICG) and poly(D,L-lactide-*co*-glycolide) (PLGA). This method was found to exhibit remarkable stability and biocompatibility features, and to provide high-quality fluorescence imaging. Furthermore, the treatment produced a greater rate of tumor cell inhibition (81.4% ± 2.1% U87 cell) *via* apoptosis. Subsequently, the researchers identified square derivative dyes that contain an oxocyclobutenate core, which exhibit a high molar absorption and robust absorption bands (Fig. 13b).[110] In 2013, Zhang conducted a research project that explored the noncovalent binding of squaraine (SQ) dyes with bovine serum albumin (BSA). The findings of this study demonstrated a considerable enhancement in fluorescence intensity, approximately ten times higher than the baseline, as well as a ten-fold increase in fluorescence lifetime. Additionally, high-quality confocal fluorescent images were obtained for HCT 116 cells landscape as potential photodynamic therapy (PDT) agents due to their remarkable attributes, including high luminescence purity, exceptional thermal and photochemical stability, and high quantum yield (Fig. 13c).[111] In 2016, Huang's research team introduced a biocompatible and highly efficient carbazole-substituted BODIPY (Car-BDP) molecule as a photosensitizer for PDT, which can penetrate deep into tissues with imaging guidance. These molecules exhibit exceptional NIR fluorescence, which enables their *in vivo* tracking and demonstrated potent tumor volume inhibition (~80%) at deep tissue levels (Fig. 13d).[112]

4.1.2. Photoimmunotherapy. NIR-photoimmunotherapy (PIT) is a novel and promising approach that integrates phototherapy and immunotherapy to effectively eliminate primary tumors, distant metastases, and prevent cancer recurrence. PIT confers distinct advantages over other therapies, such as higher efficacy and fewer side effects owing to the targeted nature of the PIT agents.[113] This innovative approach holds great

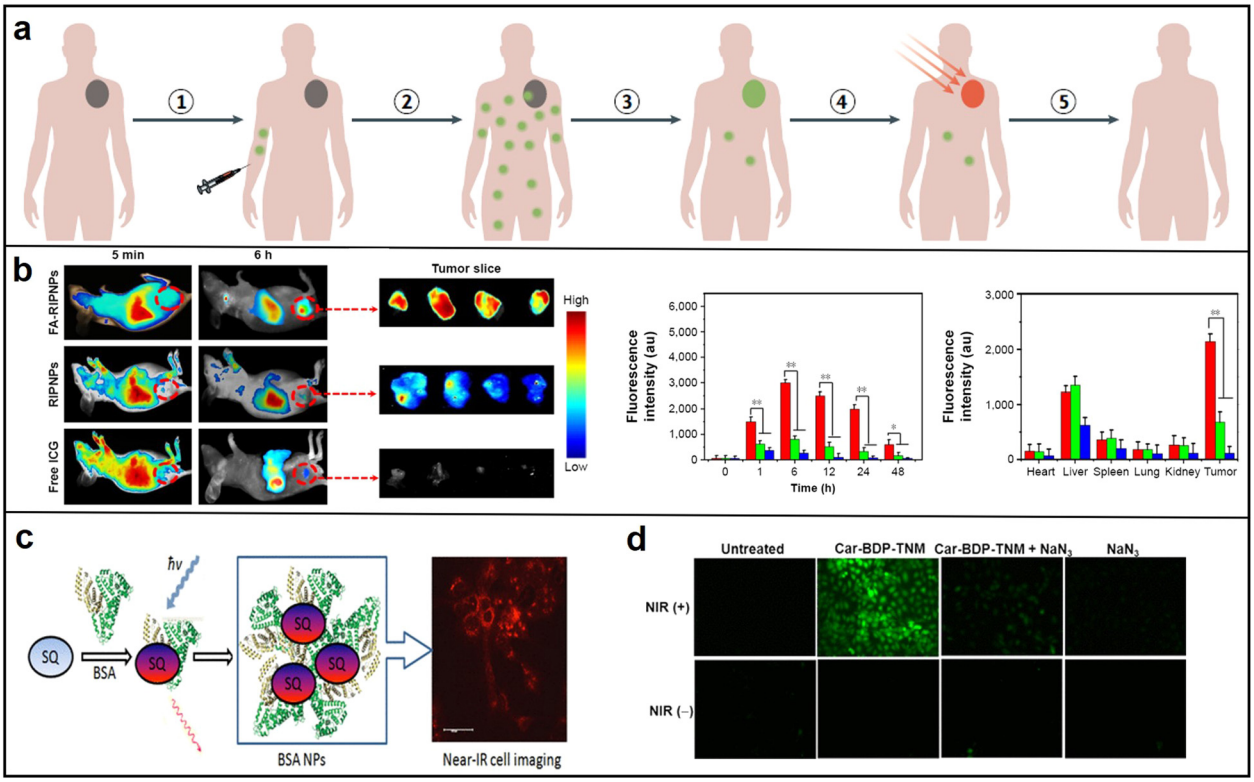

Fig. 13 (a) Schematic diagram of NIR photothermal treatment process. Reproduced with permission from ref. 104. Copyright 2020 *Nature Reviews Clinical Oncology*. (b) Representative fluorescence images of mice after tail vein injection with free ICG, RIPNPs and FA-RIPNPs (left), and quantitative *in vivo* analysis of the fluorescence signals of the tumor regions (right); reproduced with permission from ref. 110. Copyright 2016 Dove press. (c) BSA NPs and NIR cell imaging; reproduced with permission from ref. 111. Copyright 2013 *ACS Applied Materials & Interfaces*. (d) Fluorescence microscopy of singlet-oxygen generation in Car-BDP-TNM. Reproduced with permission from ref. 112. Copyright 2016 *Journal of the American Chemical Society*.

promise as a potent and highly targeted treatment option for cancer and other diseases.

Similar to PDT, PIT can also use NIR OLED as an excitation light source.[96] For photosensitizing agents, most clinical and preclinical research activities focus on administering a conjugate comprised of IRdye700DX (IR700), a NIR, water-soluble, silicon-phthalocyanine derivative, and a monoclonal antibody (mAb) that recognizes an expressed antigen on the surface of cancer cells. Recently, the mechanisms underlying cell death by these conjugate complexes have been elucidated. Initially, the mAb binds to transmembrane proteins situated on the cancer cell's surface. Subsequently, exposure to NIR light triggers photochemical ligand reactions in IR700, releasing its hydrophilic side chains and rendering the rest of the molecule highly hydrophobic. This chemical transformation results in the formation of a Z-stack multimer of silicon-phthalocyanine IR700 rings or water-insoluble aggregates of antigen-presenting cells (APCs) or APC–antigen complexes, culminating in the quenching of IR700 fluorescence. The photo-chemical ligand release reaction instigates physicochemical changes within the APC–antigen complex, compromising the transmembrane target proteins and weakening the cell membrane's integrity. This leads to an influx of water into the cell, causing cell swelling and content release. Consequently, stress markers such as heat shock proteins 70 and 90, or dying signals such as calreticulin, ATP, and HMGB1 are activated promptly, promoting the maturation of immature dendritic cells and stimulating a host immune response against the antigens released from the dying cancer cells (Fig. 14a).[113,114] Clinical trials of NIR-PIT for head and neck cancers were initiated in the United States in 2015, with the administration of RM-1929, a conjugate of IR700 and cetuximab, which targets the overexpression of EGFR in HNSCC. The results of the trials indicated that RM-1929 was safe and effective in treating locally recurrent HNSCC that cannot be surgically removed, demonstrated a superior therapeutic effect in athymic nude mouse models compared to cetuximab-based NIR-PIT, which can be attributed to its longer half-life (Fig. 14b).[115]

Panitumumab is an antibody that targets the human epidermal growth factor receptor (hEGFR) and is employed for therapeutic purposes. This study demonstrated that panitumumab-based NIR-PIT displayed enhanced therapeutic effectiveness compared to cetuximab-based NIR-PIT in athymic nude mouse models. This advantage was attributed to panitumumab's longer half-life (Fig. 14c).[116] Besides, combining two antibodies has been shown to be more effective than a single antibody–IRdye700 conjugate, resulting in improved homogeneous microdistribution. In 2021, Okada conducted research that demonstrated the superior inhibition of tumor growth through the use of a combination of two NIR-PIT reagents: panitumumab-IRdye700

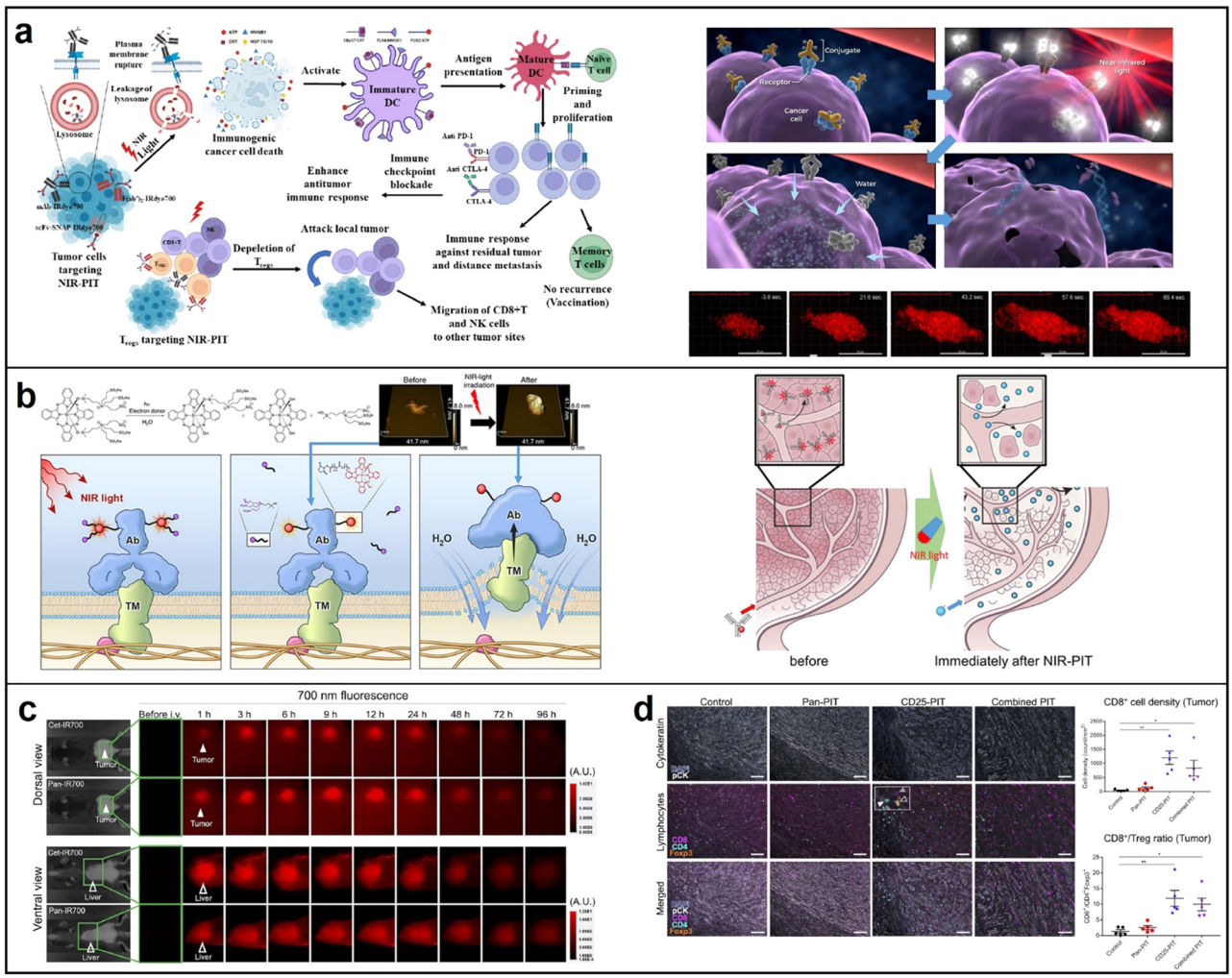

Fig. 14 (a) The principle of NIR photoimmunotherapy; reproduced with permission from ref. 113. Copyright 2023 *International Journal of Molecular Sciences*. (b) Process of RM-1929 destroying target cells (left), mechanism of super enhanced permeability and retention (SUPR) effects induced by NIR-PIT (right); reproduced with permission from ref. 115. Copyright 2021 *Head & Neck*. (c) fluorescence microscopy of tissue and liver treated with Cet-IR700 and Pan-IR700, respectively; reproduced with permission from ref. 116. Copyright 2022 *Cancer Immunology, Immunotherapy*. (d) Multiplex immunohistochemical staining of the tumors 7 days. Reproduced with permission from ref. 117. Copyright 2021 *eBioMedicine*.

and anti-CD25-F(ab0)2-IRdye700. $CD8_+$ cells showed a significantly higher density in the CD25-PIT group and in the combined PIT group compared to the control group (Fig. 14d).[117]

In conclusion, PDT and PIT have shown promise in treating specific tumors. Nevertheless, there are still challenges to overcome, such as the insufficient specificity of photosensitive materials resulting in their accumulation in normal tissues and limited efficacy for tumor cells located deeper due to the NIR light's limited penetration depth. Addressing these issues will be crucial for future research in this field.

4.2. Component determination in food industry

As the demand for nutritious foods with bioactive compounds or phytonutrients increases, researchers are exploring functional food development techniques. Effective analysis of a food's chemical components is crucial in this process. Commonly used methods such as UV spectroscopy can be costly, slow, and require complex sample preparation.[118] In contrast, NIR spectroscopy has emerged as a popular technique in the food and agriculture industry due to its intrinsic benefits such as being non-invasive, rapid, and requiring minimal sample preparation. NIR spectroscopy works based on the principle that chemical bonds such as C–H, N–H, O–H, and S–H in a sample will absorb a portion of photon energy when NIR light radiation passes through it, causing a change in the energy and frequency of the photons. The absorbed and scattered light can then be analyzed to determine the type and quantity of substances present in the sample, and to derive the sample's components and content.[119,120] This section will specifically focus on the potential applications, challenges, and opportunities of NIR spectroscopy in measuring and quantifying the functional properties of cereal and dairy food products.

4.2.1. Cereal determination. Rice and wheat are essential cereal crops that provide a significant portion of the world's

human food needs. However, during production, processing, and storage, the physicochemical properties of these crops can undergo significant changes, which can affect their quality.[121] NIR spectroscopy has emerged as an effective method for measuring the functional properties of cereal crops due to its non-invasive, rapid, and easy-to-use nature. In a study conducted by Kanitha and her team in 2016, NIR spectroscopy was utilized to develop a prediction model based on the moisture content of three types of rice stored for 31 weeks (Fig. 15a). This model accurately predicted various parameters of rice samples such as cooking time, adhesion, pasting temperature, and peak viscosity.[122] In 2018, Gergely used NIR spectroscopy to analyze the changes in physicochemical properties of wheat components during milling and heat treatments (Fig. 15b). NIR spectroscopy allowed for precise detection of various parameters, such as moisture levels and protein composition. The accurate measurements provide important information for the food industry to ensure the quality of wheat-based products, facilitating a more comprehensive understanding of the effects of processing on wheat components.[123] Furthermore, Katharina's analysis of 39 samples of vital gluten using NIR spectroscopy in 2021 revealed significant differences in the composition and variability of samples obtained from a specialized vital gluten manufacturer compared to those obtained as a by-product in the wheat starch production process (Fig. 15c).[124]

4.2.2. Dairy determination. Dairy products are assessed based on several parameters, including fatty acid content, particle size distribution, bulk density, dispersibility, and moisture content.[125] NIR spectroscopy has proven to be a useful technique for detecting these parameters. In 2020, Young utilized data pre-processing techniques and multivariate data analysis methods to integrate spectral information acquired from NIR spectroscopy of milk powder samples.[126] Regression simulations enabled the prediction of fine particle size, dispersion, and bulk weight with an accuracy of nearly 90% (Fig. 15d). In 2021, Reis and colleagues conducted a study using visible and NIR spectroscopy to analyze the physicochemical properties of dairy products from different brands, batches, and storage times.[127] They developed a partial least squares regression (PLSR) model based on spectral information to predict microstructural characteristics such as tapping density, insolubility index, and surface free fat (Fig. 15e). Besides, Anna and her team utilized NIR spectroscopy and multivariate curve resolution-alternating least squares (MCR-ALS) to investigate the effects of skim milk powder and physicochemical factors on milk coagulation (Fig. 15f). The study results revealed that increasing the concentration of reconstituted milk significantly

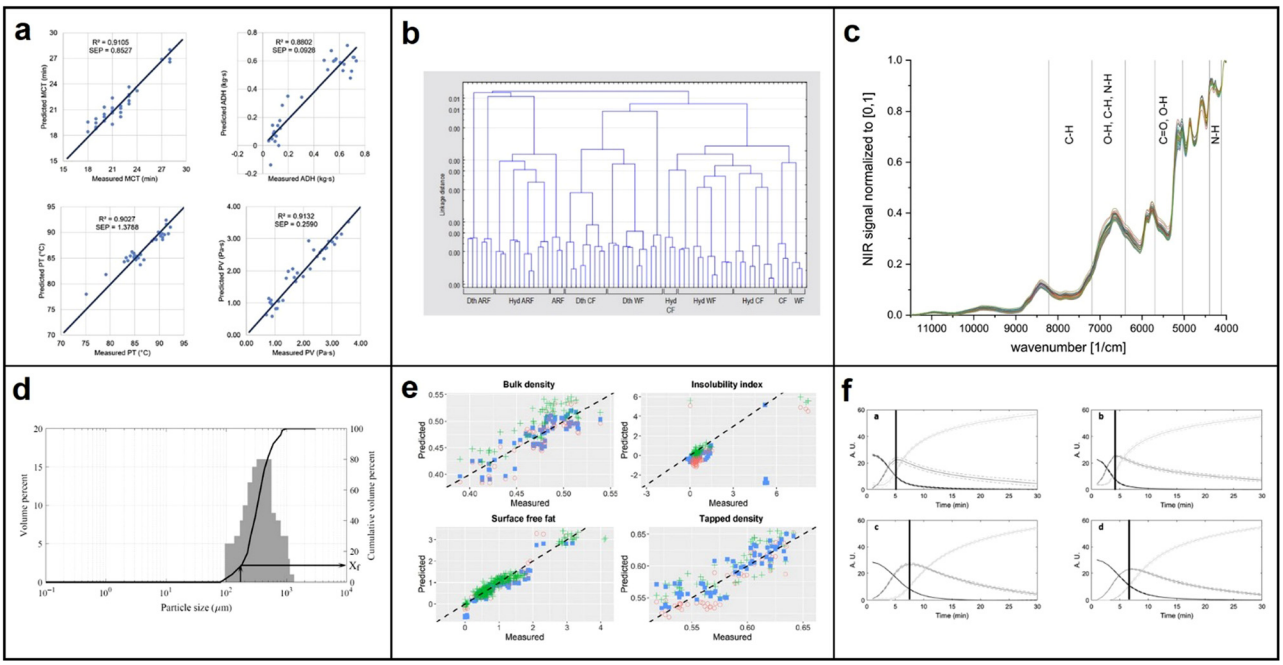

Fig. 15 (a) Comparison between NIR predicted values and measured values for selected quality parameters of validation samples; MCT = minimum cooking time; ADH = adhesiveness; PT = pasting temperature; PV = peak viscosity; reproduced with permission from ref. 122. Copyright 2016 *Journal of Cereal Science*. (b) Cluster analysis dendrogram in the case of Hungarian wheat flour (WF), Hungarian cake flour (CF) and aleurone-rich wheat flour (ARF) samples in reference to the untreated, dry-thermal treated (Dth) and hydrothermal treated (Hyd) samples in the range of 1100–2500 nm; reproduced with permission from ref. 123. Copyright 2016 *Quality Assurance and Safety of Crops & Foods*. (c) NIR spectra of vital gluten samples G1–G39; reproduced with permission from ref. 124. Copyright 2021 *European Food Research and Technology*. (d) Particle size distributions of a milk powder sample with fine particle fraction estimation from cumulative distribution curve; reproduced with permission from ref. 126. Copyright 2020 *International Journal of Dairy Technology*. (e) Scatter plots for predicted against expected values for the external validation dataset; reproduced with permission from ref. 127. Copyright 2021 *International Dairy Journal*. (f) MCR-ALS concentration profiles of coagulation trials performed with the mixtures of pasteurized skimmed milk and reconstituted milk samples: EPI 40, EPI 60, SCA 40 and SCA 60. reproduced with permission from ref. 128. Copyright 2021 *Food Control*.

reduced the coagulation time of milk powder. MCR-ALS was found to be a suitable non-invasive, non-destructive, and online tool.[128]

To summarize, NIR spectroscopy is widely utilized in the food industry because of its non-destructive, rapid, and environmentally friendly characteristics. It can effectively determine the proximate composition of food products, such as protein, moisture, dry matter, fat, and starch. Due to the generally low efficiency of NIR OLEDs, there are few reports on using them as light sources for spectrometers. However, NIR OLED has the potential to be applied in NIR spectrometer light sources due to its advantages such as lightweight, flexibility, and fast response speed.[14,21] However, further development and training are necessary to improve its ability to predict or quantify the functional properties of foods. Additionally, calibration models must be systematically established, incorporating samples from various sources and environmental conditions.[129] The integration of NIR spectroscopy with other sensing technologies, data analysis techniques, and the Internet of Things is expected to contribute significantly to the advancement of the agricultural and food industries. It should be pointed out that NIR spectroscopy can not only be applied in agricultural industry, but also in fields such as drug analysis,[130] environmental monitoring,[131] and process analytical technology.[132] With the development and innovation of technology, the application of NIR spectroscopy is constantly expanding and deepening.

5. Summary and outlook

Our review explores recent developments in organic NIR materials, devices, and applications. Specifically, we focus on molecular design strategies for efficient fluorescent, phosphorescent, and TADF emitters. These strategies involve optimizing the HOMO–LUMO energy levels, increasing conjugation length, and incorporating heavy atoms to enhance spin–orbit coupling. Notably, the design strategies vary for each type of material. For instance, efficient fluorescent materials require high quantum yields and effective energy transfer pathways, while heavy atom incorporation is essential for facilitating intersystem crossing in phosphorescent materials. In contrast, TADF materials necessitate a small energy gap between the singlet and triplet excited states to enable efficient RISC.

Design strategies for high-performing NIR OLEDs can be summarized in two aspects. On the one hand, the micro-cavity effect in OLEDs enhances OCE, resulting in a narrower emission spectrum and a potential shift in emitted light wavelength. The constructive interference of light waves at specific wavelengths boosts the amount of emitted light, leading to improved color purity and accuracy. What's even more remarkable is that controlling the microcavity effect can be achieved simply by adjusting the device thickness, which is a highly efficient and low-cost device development strategy. On the other hand, optimizing charge balance and carrier injection/transport properties can reduce energy loss due to non-radiative processes, which can further improve device efficiency and stability.

NIR materials and OLEDs have a wide range of potential applications in biomedical and component determination. NIR fluorescence imaging, for instance, has the ability to detect and monitor tumors non-invasively in biological tissues. Furthermore, NIR spectroscopy can be used for the chemical analysis of components in various fields, such as food quality control and environmental monitoring. Nonetheless, there are limitations to these applications. For example, the accuracy and resolution of imaging may be affected by the limited penetration depth of NIR light in biological tissues due to absorption and scattering. Additionally, the stability and toxicity of NIR materials must be thoroughly considered for biomedical applications.

Despite the limitations, the future prospects for the development of NIR materials, devices, and applications are exciting. Advances in nanotechnology and biocompatible materials offer the potential for improved imaging resolution and sensitivity. Furthermore, the development of flexible OLEDs holds promise for new applications in wearable devices and displays.

Conflicts of interest

There are no conflicts to declare.

Acknowledgements

This work was supported by the National Natural Science Foundation of China (Grant No. 62174067, 62175085), Science and Technology Development Planning of Jilin Province (Project No. 20230101061JC) and Open Project of Key Lab of Special Functional Materials of Ministry of Education, Henan University (KFKT-2022-01).

References

1 J. Zhang, H. R. Ye, Y. X. Jin and D. M. Han, Recent progress in near-infrared organic electroluminescent materials, *Top. Curr. Chem.*, 2022, **380**, 6.
2 D. Liu, G. Li, P. Dang, Q. Zhang, Y. Wei, L. Qiu, M. S. Molokeev, H. Lian, M. Shang and J. Lin, Highly efficient Fe^{3+}-doped A2BB′O6 (A = Sr^{2+}, Ca^{2+}; B, B′ = In^{3+}, Sb^{5+}, Sn^{4+}) broadband near-infrared-emitting phosphors for spectroscopic analysis, *Light Sci. Appl.*, 2022, **11**, 112.
3 J. Ackermann, J. T. Metternich, S. Herbertz and S. Kruss, Biosensing with fluorescent carbon nanotubes, *Angew. Chem., Int. Ed.*, 2022, **61**, e202112372.
4 A. A. Ansari, A. K. Parchur and G. Chen, Surface modified lanthanide upconversion nanoparticles for drug delivery, cellular uptake mechanism, and current challenges in NIR-driven therapies, *Coord. Chem. Rev.*, 2022, **457**, 214423.
5 F. Fang, Y. Yuan, Y. Wan, J. Li, Y. Song, W. C. Chen, D. Zhao, Y. Chi, M. Li, C. S. Lee and J. Zhang, Near-infrared thermally activated delayed fluorescence nanoparticle: a metal-free photosensitizer for two-photon-activated

photodynamic therapy at the cell and small animal levels, *Small*, 2022, **18**, 2106215.

6 M. Y. Zhao, B. H. Li, Y. F. Wu, H. S. He, X. Y. Zhu, H. X. Zhang, C. R. Dou, L. S. Feng, Y. Fan and F. Zhang, A tumor-microenvironment-responsive lanthanide-cyanine FRET sensor for NIR-II luminescence-lifetime in situ imaging of hepatocellular carcinoma, *Adv. Mater.*, 2020, **32**, 2001172.

7 L. Feng, C. Li, L. Liu, Z. Wang, Z. Chen, J. Yu, W. Ji, G. Jiang, P. Zhang, J. Wang and B. Z. Tang, Acceptor planarization and donor rotation: a facile strategy for realizing synergistic cancer phototherapy via type I PDT and PTT, *ACS Nano*, 2022, **16**, 4162–4174.

8 H. Li, H. Kim, F. Xu, J. Han, Q. Yao, J. Wang, K. Pu, X. Peng and J. Yoon, Activity-based NIR fluorescent probes based on the versatile hemicyanine scaffold: design strategy, biomedical applications, and outlook, *Chem. Soc. Rev.*, 2022, **51**, 1795–1835.

9 T. Basile, A. D. Marsico and R. Perniola, Use of artificial neural networks and NIR spectroscopy for non-destructive grape texture prediction, *Foods*, 2022, **11**, 281.

10 F. Zhao, Z. Song and Q. Liu, Advances in chromium-activated phosphors for near-infrared light sources, *Laser Photonics Rev.*, 2022, **16**, 2200380.

11 Y. C. Wei, S. F. Wang, Y. Hu, L. S. Liao, D. G. Chen, K. H. Chang, C. W. Wang, S. H. Liu, W. H. Chan, J. L. Liao, W. Y. Hung, T. H. Wang, P. T. Chen, H. F. Hsu, Y. Chi and P. T. Chou, Overcoming the energy gap law in near-infrared OLEDs by exciton-vibration decoupling, *Nat. Photonics*, 2020, **14**, 570–577.

12 D. M. Xi, M. Xiao, J. F. Cao, L. Y. Zhao, N. Xu, S. R. Long, J. L. Fan, K. Shao, W. Sun and X. H. Yan, NIR Light-Driving Barrier-Free Group Rotation in Nanoparticles with an 88.3% Photothermal Conversion Efficiency for Photothermal Therapy, *Adv. Mater.*, 2020, **32**, 1907855.

13 Q. X. Dang, Y. Y. Jiang, J. F. Wang, J. Q. Wang, Q. H. Zhang, M. K. Zhang, S. M. Luo, Y. J. Xie, K. Y. Pu and Q. Q. Li, Room-temperature phosphorescence resonance energy transfer for construction of near-infrared afterglow imaging agents, *Adv. Mater.*, 2020, **32**, 2006752.

14 Q. Y. Zhang, M. X. Xu, L. M. Zhou, S. H. Liu, W. Wang, L. T. Zhang, W. F. Xie and C. J. Yu, A flexible organic mechanoluminophore device, *Nat. Commun.*, 2023, **14**, 1257.

15 T. Pan, S. H. Liu, L. T. Zhang, W. F. Xie and C. J. Yu, A flexible, multifunctional, optoelectronic anticounterfeiting device from high-performance organic light-emitting paper, *Light: Sci. Appl.*, 2022, **11**, 59.

16 S. H. Liu, J. M. Zhang, C. X. Zang, L. T. Zhang, W. F. Xie and C. S. Lee, Centimeter-scale hole diffusion and its application in organic light-emitting diodes, *Sci. Adv.*, 1999, **8**, eabm1999.

17 C. X. Zang, S. H. Liu, M. X. Xu, R. F. Wang, C. Cao, Z. L. Zhu, J. M. Zhang, H. Wang, L. T. Zhang, W. F. Xie and C. S. Lee, Top-emitting thermally activated delayed fluorescence organic light-emitting devices with weak light-matter coupling, *Light: Sci. Appl.*, 2021, **10**, 116.

18 M. Y. Wong and E. Zysman-Colman, Purely organic thermally activated delayed fluorescence materials for organic light-emitting diodes, *Adv. Mater.*, 2017, **29**, 1605444.

19 Z. Yu, Q. Y. Li, Q. Ma, W. P. Ye, Z. F. An and H. L. Ma, Excited-state descriptors for high-throughput screening of efficient electro-fluorescent materials, *Chem. Mater.*, 2023, **35**, 1827–1833.

20 Y. Z. Shi, H. Wu, K. Wang, J. Yu, X. M. Ou and X. H. Zhang, Recent progress in thermally activated delayed fluorescence emitters for nondoped organic light-emitting diodes, *Chem. Sci.*, 2022, **13**, 3625–3651.

21 G. Y. Zhang, D. Y. Wang, B. B. Lou, C. G. Ma and Y. H. Wang, Efficient broadband near-infrared emission from lead-free halide double perovskite single crystal, *Angew. Chem. Int. Ed.*, 2022, **61**, e202207454.

22 Q. Wang, W. X. Dai, Y. L. Xie, Q. Q. Ke, C. H. Zhao, B. Zhang, Z. B. Zeng, Z. M. Wang and B. Z. Tang, AIE-active deep red/near-infrared electroluminescent emitters with fine regulation of excited state, *Chem. Eng. J.*, 2022, **451**, 138529.

23 C. You, D. Liu, M. Zhu, J. Yu, B. Zhang, Y. Liu, Y. Wang and W. Zhu, Σ–π and p–π conjugation induced NIR-emitting iridium(III) complexes anchored by flexible side chains in a rigid dibenzo[a,c]phenazine moiety and their application in highly efficient solution-processable NIR-emitting devices, *J. Mater. Chem. C*, 2020, **8**, 7079–7088.

24 X. Zhong, T. Chervy, L. Zhang, A. Thomas, J. George, C. Genet, J. A. Hutchison and T. W. Ebbesen, Energy transfer between spatially separated entangled molecules, *Angew. Chem., Int. Ed.*, 2017, **56**, 9034–9038.

25 S. H. Liu, C. X. Zang, J. M. Zhang, S. Tian, Y. Wu, D. Shen, L. T. Zhang, W. F. Xie and C. S. Lee, Air-stable ultrabright inverted organic light-emitting devices with metal ion-chelated polymer injection layer, *Nanomicro Lett.*, 2021, **14**, 14.

26 C. X. Zang, M. X. Xu, L. T. Zhang, S. H. Liu and W. F. Xie, Organic–inorganic hybrid thin film light-emitting devices: Interfacial engineering and device physics, *J. Mater. Chem. C*, 2021, **9**, 1484–1519.

27 J. M. Zhang, S. A. Liu, Y. F. Chen, L. T. Zhang and W. F. Xie, Simple-structure color-tunable fluorescent organic light-emitting devices with chromaticity difference beyond five-step mcadam ellipses, *J. Phys. D*, 2021, **54**, 505103.

28 U. Balijapalli, R. Nagata, N. Yamada, H. Nakanotani, M. Tanaka, A. D'Aleo, V. Placide, M. Mamada, Y. Tsuchiya and C. Adachi, Highly efficient near-infrared electrofluorescence from a thermally activated delayed fluorescence molecule, *Angew. Chem., Int. Ed.*, 2021, **60**, 8477–8482.

29 C. F. You, D. H. Liu, J. T. Yu, H. Tan, M. B. Zhu, B. Zhang, Y. Liu, Y. F. Wang and W. G. Zhu, Boosting efficiency of near-infrared emitting iridium(III) phosphors by administrating their pi-pi conjugation effect of core-shell structure in solution-processed OLEDs, *Adv. Opt. Mater.*, 2020, **8**, 2000154.

30 S. F. Wang, Y. Yuan, Y. C. Wei, W. H. Chan, L. W. Fu, B. K. Su, I. Y. Chen, K. J. Chou, P. T. Chen, H. F. Hsu,

C. L. Ko, W. Y. Hung, C. S. Lee, P. T. Chou and Y. Chi, Highly efficient near-infrared electroluminescence up to 800 nm using platinum(II) phosphors, *Adv. Funct. Mater.*, 2020, **30**, 2002173.

31 A. Shahalizad, A. Malinge, L. Hu, G. Laflamme, L. Haeberle, D. M. Myers, J. Mao, W. G. Skene and S. Kena-Cohen, Efficient solution-processed hyperfluorescent OLEDs with spectrally narrow emission at 840 nm, *Adv. Funct. Mater.*, 2021, **31**, 2007119.

32 C. Y. Sun, X. Z. Wang, Y. M. Xu, W. B. Lu, X. Y. Teng, G. S. Fu and W. Yu, Physical origins of high photoluminescence quantum yield in alpha-$CsPbI_3$ nanocrystals and their stability, *Appl. Surf. Sci.*, 2020, **508**, 145188.

33 Y. Y. Wang, T. E. Hsieh, I. C. Chen and C. H. Chen, Direct encapsulation of organic light-emitting devices (OLEDs) using photo-curable co-polyacrylate/silica nanocomposite resin, *IEEE Trans. Adv. Packag.*, 2007, **30**, 421–427.

34 H. U. Kim, T. Kim, C. Kim, M. Kim and T. Park, Recent advances in structural design of efficient near-infrared light-emitting organic small molecules, *Adv. Funct. Mater.*, 2022, **33**, 202208082.

35 C. T. Jackson, S. Jeong, G. F. Dorlhiac and M. P. Landry, Advances in engineering near-infrared luminescent materials, *Iscience*, 2021, **24**, 102156.

36 S. T. Le, T. Kanesan, F. Bausi, P. A. Haigh, S. Rajbhandari, Z. Ghassemlooy, I. Papakonstantinou, W. O. Popoola, A. Burton, H. Le Minh, F. Cacialli and A. D. Ellis, 10 Mb/s visible light transmission system using a polymer light-emitting diode with orthogonal frequency division multiplexing, *Opt. Lett.*, 2014, **39**, 3876–3879.

37 P. A. Haigh, F. Bausi, Z. Ghassemlooy, I. Papakonstantinou, H. Le Minh, C. Fléchon and F. Cacialli, Visible light communications: Real time 10 Mb/s link with a low bandwidth polymer light-emitting diode, *Opt. Express*, 2014, **22**, 2830–2838.

38 G. Qian, Z. Zhong, M. Luo, D. Yu, Z. Zhang, Z. Y. Wang and D. Ma, Simple and efficient near-infrared organic chromophores for light-emitting diodes with single electroluminescent emission above 1000 nm, *Adv. Mater.*, 2009, **21**, 111–116.

39 S. Ellinger, K. R. Graham, P. Shi, R. T. Farley, T. T. Steckler, R. N. Brookins, P. Taranekar, J. Mei, L. A. Padilha, T. R. Ensley, H. Hu, S. Webster, D. J. Hagan, E. W. Van Stryland, K. S. Schanze and J. R. Reynolds, Donor–acceptor–donor-based π-conjugated oligomers for nonlinear optics and near-IR emission, *Chem. Mater.*, 2011, **23**, 3805–3817.

40 A. Zampetti, A. Minotto, B. M. Squeo, V. G. Gregoriou, S. Allard, U. Scherf, C. L. Chochos and F. Cacialli, Highly efficient solid-state near-infrared organic light-emitting diodes incorporating A–D–A dyes based on α,β-unsubstituted "bodipy" moieties, *Sci. Rep.*, 2017, **7**, 1611.

41 J. Zhang, L. Xu, C. L. Ho and W. Y. Wong, Functional organometallic poly(arylene ethynylene)s: from synthesis to applications, *Top. Curr. Chem.*, 2017, **375**, 17.

42 S. Tang, P. Murto, X. Xu, C. Larsen, E. Wang and L. Edman, Intense and stable near-infrared emission from light-emitting electrochemical cells comprising a metal-free indacenodithieno [3,2-b]thiophene-based copolymer as the single emitter, *Chem. Mater.*, 2017, **29**, 7750–7759.

43 P. Murto, A. Minotto, A. Zampetti, X. Xu, M. R. Andersson, F. Cacialli and E. Wang, Triazolobenzothiadiazole-based copolymers for polymer light-emitting diodes: pure near-infrared emission via optimized energy and charge transfer, *Adv. Opt. Mater.*, 2016, **4**, 2068–2076.

44 G. Tregnago, T. T. Steckler, O. Fenwick, M. R. Andersson and F. Cacialli, Thia- and selena-diazole containing polymers for near-infrared light-emitting diodes, *J. Mater. Chem. C*, 2015, **3**, 2792–2797.

45 O. Fenwick, J. K. Sprafke, J. Binas, D. V. Kondratuk, F. Di Stasio, H. L. Anderson and F. Cacialli, Linear and cyclic porphyrin hexamers as near-infrared emitters in organic light-emitting diodes, *Nano Lett.*, 2011, **11**, 2451–2456.

46 Z. Zhao, H. K. Zhang, J. W. Y. Lam and B. Z. Tang, Aggregation-induced emission: new vistas at the aggregate level, *Angew. Chem., Int. Ed.*, 2020, **59**, 9888–9907.

47 Z. Wang, L. Yan, L. Zhang, Y. Chen, H. Li, J. Zhang, Y. Zhang, X. Li, B. Xu, X. Fu, Z. Sun and W. Tian, Ultra bright red AIE dots for cytoplasm and nuclear imaging, *Polym. Chem.*, 2014, **5**, 7013–7020.

48 A. D. Shao, Y. S. Xie, S. J. Zhu, Z. Q. Guo, S. Q. Zhu, J. Guo, P. Shi, T. D. James, H. Tian and W. H. Zhu, Far-red and near-IR AIE-active fluorescent organic nanoprobes with enhanced tumor-targeting efficacy: shape-specific effects, *Angew. Chem., Int. Ed.*, 2015, **54**, 7275–7280.

49 J. Luo, X. F. Rong, Y. Y. Ye, W. Z. Li, X. Q. Wang and W. J. Wang, Research progress on triarylmethyl radical-based high-efficiency OLED, *Molecules*, 2022, **27**, 1632.

50 F. C. Zhao, Y. Wei, H. Xu, D. Chen, T. Ahamad, S. Alshehri, Q. B. Pei and D. G. Ma, Spatial exciton allocation strategy with reduced energy loss for high-efficiency fluorescent/phosphorescent hybrid white organic light-emitting diodes, *Mater. Horiz.*, 2017, **4**, 641–648.

51 H. T. Kim, K. Lee, W. Jin, H. D. Um, M. Lee, E. Hwang, T. H. Kwon and K. Seo, Phosphorescent energy down-shifting for diminishing surface recombination in silicon nanowire solar cells, *Sci. Rep.*, 2018, **8**, 16974.

52 J. Zhang, H. Ye, Y. Jin and D. Han, Recent progress in near-infrared organic electroluminescent materials, *Top. Curr. Chem.*, 2021, **380**, 6.

53 X. L. Yang, G. J. Zhou and W. Y. Wong, Functionalization of phosphorescent emitters and their host materials by main-group elements for phosphorescent organic light-emitting devices, *Chem. Soc. Rev.*, 2015, **44**, 8484–8575.

54 S. Y. Yang, F. Y. Meng, X. G. Wu, Z. Yin, X. Z. Liu, C. F. You, Y. F. Wang, S. J. Su and W. G. Zhu, Dinuclear platinum(II) complex dominated by a zig-zag-type cyclometalated ligand: a new approach to realize high-efficiency near infrared emission, *J. Mater. Chem. C*, 2018, **6**, 5769–5777.

55 X. L. Yang, B. Jiao, J. S. Dang, Y. H. Sun, Y. Wu, G. J. Zhou and W. Y. Wong, Achieving high-performance solution-processed orange OLEDs with the phosphorescent cyclometalated

trinuclear Pt(II) complex, *ACS Appl. Mater. Interfaces*, 2018, **10**, 10227–10235.

56 H. T. Kidanu, J. H. Lee and C.-T. Chen, Photoluminescence and electroluminescence characterization of high-performance near-infrared emitters based on 1,5-naphthyridin-4-ol-containing heteroleptic platinum(II) complexes, *Mater. Adv.*, 2021, **2**, 3589–3599.

57 Y. M. Zhang, F. Y. Meng, J. H. Tang, Y. F. Wang, C. F. You, H. Tan, Y. Liu, Y. W. Zhong, S. J. Su and W. G. Zhu, Achieving near-infrared emission in platinum(II) complexes by using an extended donor-acceptor-type ligand, *Dalton Trans.*, 2016, **45**, 5071–5080.

58 F. Nisic, A. Colombo, C. Dragonetti, D. Roberto, A. Valore, J. M. Malicka, M. Cocchi, G. R. Freeman and J. A. G. Williams, Platinum(II) complexes with cyclometallated 5-π-delocalized-donor-1,3-di(2-pyridyl)benzene ligands as efficient phosphors for NIR-OLEDs, *J. Mater. Chem. C*, 2014, **2**, 1791–1800.

59 L. Yang, J. Hu, W. Zeng, Y. Wu, X. Li, D. Zhang and W. Jin, Synthesis, self-assemble and fluorescence of pyrimidine-contained novel rod-coil structured n^c^n-type divalent platium complexes, *Chinese J. Org. Chem.*, 2017, **37**, 2647–2654.

60 G. Y. Pan, H. R. Jia, Y. X. Zhu and F. G. Wu, Turning double hydrophilic into amphiphilic: Ir825-conjugated polymeric nanomicelles for near-infrared fluorescence imaging-guided photothermal cancer therapy, *Nanoscale*, 2018, **10**, 2115–2127.

61 L. Huang, C. D. Park, T. Fleetham and J. Li, Platinum(II) azatetrabenzoporphyrins for near-infrared organic light emitting diodes, *Appl. Phys. Lett.*, 2016, **109**, 233302.

62 Y. Zhang, F. Meng, C. You, S. Yang, L. Xiong, W. Xiong, W. Zhu, Y. Wang, Y. Pei and S. Su, Efficient near-infrared emitting tetradentate bis-cyclometalated platinum(IV) complexes for solution-processed polymer light-emitting diodes, *Dyes Pigm.*, 2017, **142**, 457–464.

63 B. Blondel, A. Colin, M. Lopes, F. Alary, G. Zissis, I. Sasaki and C. Renaud, Application of [Pt(II)(tetra-tert-butyl-salophen)] complex within organic devices: deep red emission, bistable light-emitting diodes and operational stability, *Appl. Sci.*, 2018, **8**, 762.

64 N. Su, F. Meng, P. Wang, X. Liu, M. Zhu, W. Zhu, S. Su and J. Yu, Near-infrared emission from binuclear platinum (II) complexes containing pyrenylpyridine and pyridylthiolate units: synthesis, photo-physical and electroluminescent properties, *Dyes Pigm.*, 2017, **138**, 162–168.

65 M. Z. Shafikov, P. Pander, A. V. Zaytsev, R. Daniels, R. Martinscroft, F. B. Dias, J. A. G. Williams and V. N. Kozhevnikov, Extended ligand conjugation and dinuclearity as a route to efficient platinum-based near-infrared (NIR) triplet emitters and solution-processed NIR-OLEDs, *J. Mater. Chem. C*, 2021, **9**, 127–135.

66 C. L. Ho, W. Y. Wong, G. J. Zhou, B. Yao, Z. Xie and L. Wang, Solution-processible multi-component cyclometalated Iridium phosphors for high-efficiency orange-emitting OLEDs and their potential use as white light sources, *Adv. Funct. Mater.*, 2007, **17**, 2925–2936.

67 J. Xue, L. Xin, J. Hou, L. Duan, R. Wang, Y. Wei and J. Qiao, Homoleptic facial ir(III) complexes via facile synthesis for high-efficiency and low-roll-off near-infrared organic light-emitting diodes over 750 nm, *Chem. Mater.*, 2017, **29**, 4775–4782.

68 Y. Liu, Z. Hao, F. Meng, P. Wang, L. Yang, Y. Wang, Y. Pei and S. Su, Efficient near-infrared emission of π-extended cyclometalated iridium complexes based on pyrene in solution-processed polymer light-emitting diode, *Chem. Phys. Lett.*, 2018, **699**, 99–106.

69 H. U. Kim, H. J. Jang, W. Choi, S. Park, T. Park, J. Y. Lee and K. S. Bejoymohandas, Aggregation-induced phosphorescence enhancement in deep-red and near-infrared emissive iridium(III) complexes for solution-processable OLEDs, *J. Mater. Chem. C*, 2020, **8**, 4789–4800.

70 X. K. Chen, D. Kim and J. L. Bredas, Thermally activated delayed fluorescence (TADF) path toward efficient electroluminescence in purely organic materials: molecular level insight, *Acc. Chem. Res.*, 2018, **51**, 2215–2224.

71 X. K. Liu, Z. Chen, J. Qing, W. J. Zhang, B. Wu, H. L. Tam, F. R. Zhu, X. H. Zhang and C. S. Lee, Remanagement of singlet and triplet excitons in single-emissive-layer hybrid white organic light-emitting devices using thermally activated delayed fluorescent blue exciplex, *Adv. Mater.*, 2015, **27**, 7079.

72 K. H. Kim, S. J. Yoo and J. J. Kim, Boosting triplet harvest by reducing nonradiative transition of exciplex toward fluorescent organic light-emitting diodes with 100% internal quantum efficiency, *Chem. Mater.*, 2016, **28**, 1936–1941.

73 C. Li, L. Duan, D. D. Zhang and Y. Qiu, Thermally activated delayed fluorescence sensitized phosphorescence: a strategy to break the trade-off between efficiency and efficiency roll-off, *ACS Appl. Mater. Interfaces*, 2015, **7**, 15154–15159.

74 Y. Z. Shi, H. Wu, K. Wang, J. Yu, X. M. Ou and X. H. Zhang, Recent progress in thermally activated delayed fluorescence emitters for nondoped organic light-emitting diodes, *Chem. Sci.*, 2022, **13**, 3625–3651.

75 B. Zhao, H. Wang, C. Han, P. Ma, Z. Li, P. Chang and H. Xu, Highly efficient deep-red non-doped diodes based on a t-shape thermally activated delayed fluorescence emitter, *Angew. Chem., Int. Ed.*, 2020, **59**, 19042–19047.

76 Z. Y. Cai, X. Wu, H. Liu, J. J. Guo, D. Z. Yang, D. G. Ma, Z. J. Zhao and B. Z. Tang, Realizing record-high electroluminescence efficiency of 31.5% for red thermally activated delayed fluorescence molecules, *Angew. Chem., Int. Ed.*, 2021, **60**, 23635–23640.

77 Y. G. Zhang, D. D. Zhang, M. H. Cai, Y. L. Li, D. Q. Zhang, Y. Qiu and L. Duan, Towards highly efficient red thermally activated delayed fluorescence materials by the control of intra-molecular π–π stacking interactions, *Nanotechnology*, 2016, **27**, 094001.

78 S. Wang, X. Yan, Z. Cheng, H. Zhang, Y. Liu and Y. Wang, Highly efficient near-infrared delayed fluorescence organic light emitting diodes using a phenanthrene-based charge-transfer compound, *Angew. Chem., Int. Ed.*, 2015, **54**, 13068–13072.

79 Y. J. Yu, Y. Hu, S. Y. Yang, W. Luo, Y. Yuan, C. C. Peng, J. F. Liu, A. Khan, Z. Q. Jiang and L. S. Liao, Near-infrared electroluminescence beyond 800 nm with high efficiency and radiance from anthracene cored emitters, *Angew. Chem., Int. Ed.*, 2020, **59**, 21578–21584.
80 U. Balijapalli, R. Nagata, N. Yamada, H. Nakanotani, M. Tanaka, A. D'Aléo, V. Placide, M. Mamada, Y. Tsuchiya and C. Adachi, Highly efficient near-infrared electrofluorescence from a thermally activated delayed fluorescence molecule, *Angew. Chem., Int. Ed.*, 2021, **60**, 8477–8482.
81 H. Wang, B. Zhao, C. Qu, C. Duan, Z. Li, P. Ma, P. Chang, C. Han and H. Xu, 2,3-dicyanopyrazino phenanthroline enhanced charge transfer for efficient near-infrared thermally activated delayed fluorescent diodes, *Chem. Eng. J.*, 2022, **436**, 135080.
82 J. L. He, Y. Tang, K. Zhang, Y. Zhao, Y. C. Lin, C. K. Hsu, C. H. Chen, T. L. Chiu, J. H. Lee, C. K. Wang, C. C. Wu and J. Fan, An extended π-backbone for highly efficient near-infrared thermally activated delayed fluorescence with enhanced horizontal molecular orientation, *Mater. Horiz.*, 2022, **9**, 772–779.
83 H. Ye, D. H. Kim, X. Chen, A. S. D. Sandanayaka, J. U. Kim, E. Zaborova, G. Canard, Y. Tsuchiya, E. Y. Choi, J. W. Wu, F. Fages, J. L. Bredas, A. D'Aléo, J. C. Ribierre and C. Adachi, Near-infrared electroluminescence and low threshold amplified spontaneous emission above 800 nm from a thermally activated delayed fluorescent emitter, *Chem. Mater.*, 2018, **30**, 6702–6710.
84 F. Liu, Y. Tan, H. Liu, X. Tang, L. Gao, C. Du, J. Min, H. Jin and P. Lu, High-efficiency near-infrared fluorescent organic light-emitting diodes with small efficiency roll-off based on AIE-active phenanthro[9,10-d]imidazole derivatives, *J. Mater. Chem. C*, 2020, **8**, 6883–6890.
85 C. W. Tang and S. A. VanSlyke, Organic electroluminescent diodes, *Appl. Phys. Lett.*, 1987, **51**, 913–915.
86 H. Wang, H. Y. Zhao, C. X. Zang, S. H. Liu, L. T. Zhang and W. F. Xie, Stable and efficient phosphorescent organic light-emitting device utilizing a δ-carboline-containing host displaying thermally activated delayed fluorescence, *J. Mater. Chem. C*, 2020, **8**, 3800–3806.
87 S. H. Liu, Y. C. Wang, C. M. Chang, T. Yasuda, N. Fukui, H. Maeda, P. Long, K. Nakazato, W. B. Jian, W. F. Xie, K. Tsukagoshi and H. Nishihara, Solution-processed organometallic quasi-two-dimensional nanosheets as a hole buffer layer for organic light-emitting devices, *Nanoscale*, 2020, **12**, 6983–6990.
88 C. X. Zang, H. Wang, S. H. Liu, W. B. Guo, L. T. Zhang and W. F. Xie, Efficiency enhancement in an inverted organic light-emitting device with a TiO_2 electron injection layer through interfacial engineering, *J. Mater. Chem. C*, 2020, **8**, 8206–8212.
89 C. X. Zang, X. M. Peng, H. Wang, Z. W. Yu, L. T. Zhang, W. F. Xie and H. Y. Zhao, Efficient multilayer and single layer phosphorescent organic lightemitting devices using a host with balanced bipolar transporting properties and appropriate energy level, *Org. Electron.*, 2017, **50**, 106–114.
90 H. W. Yu, J. M. Zhang, T. Long, M. X. Xu, H. W. Feng, L. T. Zhang, S. H. Liu and W. F. Xie, Efficient all-blade-coated quantum dot light-emitting diodes through solvent engineering, *J. Phys. Chem. Lett.*, 2020, **11**, 9019–9025.
91 S. H. Liu, X. Zhang, M. J. Yin, H. W. Feng, J. M. Zhang, L. T. Zhang and W. F. Xie, Coffee-ring-free ultrasonic spray coating single-emission layers for white organic light-emitting devices and their energy-transfer mechanism, *ACS Appl. Energy Mater.*, 2018, **1**, 103–112.
92 C. Murawski, K. Leo and M. C. Gather, Efficiency roll-off in organic light-emitting diodes, *Adv. Mater.*, 2013, **25**, 6801–6827.
93 A. Salehi, X. Fu, D.-H. Shin and F. So, Recent advances in OLED optical design, *Adv. Funct. Mater.*, 2019, **29**, 1808803.
94 Z. W. Yu, J. M. Zhang, S. H. Liu, L. T. Zhang, Y. Zhao, H. W. Zhao and W. F. Xie, High-efficiency blue phosphorescent organic light-emitting devices with low efficiency roll-off at ultrahigh luminance by the reduction of triplet-polaron quenching, *ACS Appl. Mater. Interfaces*, 2019, **11**, 6292–6301.
95 X. Gong, C. H. Lu, W. K. Lee, P. Li, Y. H. Huang, Z. X. Chen, L. S. Zhan, C. C. Wu, S. L. Gong and C. L. Yang, High-efficiency red thermally activated delayed fluorescence emitters based on benzothiophene-fused spiro-acridine donor, *Chem. Eng. J.*, 2021, **405**, 126663.
96 Y. Park, H. R. Choi, Y. Jeon, H. Kim, J. W. Shin, C. H. Huh, K. C. Park and K. C. Choi, Cell proliferation effect of deep-penetrating microcavity tandem NIR OLEDs with therapeutic trend analysis, *Sci. Rep.*, 2022, **12**, 10935.
97 Y. S. Chen, D. Luo, W. C. Wei, B. L. Chen, T. H. Yeh, S. W. Liu and K. T. Wong, New exciplex-forming co-host system and thienothiadazole-based fluorescent emitter for high-efficiency and promising stability near-infrared OLED, *Adv. Opt. Mater.*, 2022, **10**, 2101952.
98 J. Xu, F. Peng, Z. Sun, L. Yu, W. Yang and Y. Cao, Near-infrared polymer light-emitting diodes based on an inverted device structure, *J. Mater. Chem. C*, 2019, **7**, 12114–12120.
99 R. Nagata, H. Nakanotani, W. J. Potscavage Jr and C. Adachi, Exploiting singlet fission in organic light-emitting diodes, *Adv. Mater.*, 2018, **30**, 1801484.
100 T. Yamanaka, H. Nakanotani, S. Hara, T. Hirohata and C. Adachi, Near-infrared organic light-emitting diodes for biosensing with high operating stability, *Appl. Phys. Express*, 2017, **10**, 074101.
101 A. Shahalizad, D. H. Kim, S. Rao Bobbara, Y. Tsuchiya, A. D'Aléo, C. Andraud, J. C. Ribierre, J. M. Nunzi and C. Adachi, Enhanced near-infrared electroluminescence from a Neodymium complex in organic light-emitting diodes with a solution-processed exciplex host, *Appl. Phys. Lett.*, 2019, **114**, 033301.
102 S. Hofmann, M. Thomschke, B. Luessem and K. Leo, Top-emitting organic light-emitting diodes, *Opt. Express*, 2011, **19**, A1250–A1264.
103 Y. C. Wei, S. F. Wang, Y. Hu, L. S. Liao, D. G. Chen, K. H. Chang, C. W. Wang, S. H. Liu, W. H. Chan and J. L. Liao, Overcoming the energy gap law in near-infrared

OLEDs by exciton-vibration decoupling, *Nat. Photonics*, 2022, **14**, 570–577.

104 X. S. Li, J. F. Lovell, J. Yoon and X. Y. Chen, Clinical development and potential of photothermal and photodynamic therapies for cancer, *Nat. Rev. Clin. Oncol.*, 2020, **17**, 657–674.

105 X. Jiang, B. Du, Y. Huang, M. Yu and J. Zheng, Cancer photothermal therapy with ICG-conjugated gold nanoclusters, *Bioconjugate Chem.*, 2020, **31**, 1522–1528.

106 D. E. J. G. J. Dolmans, D. Fukumura and R. K. Jain, Photodynamic therapy for cancer, *Nat. Rev. Cancer*, 2003, **3**, 380–387.

107 R. Ackroyd, C. Kelty, N. Brown and M. Reed, The history of photodetection and photodynamic therapy, *Photochem. Photobiol.*, 2001, **74**, 656–669.

108 Y. Liu, P. Bhattarai, Z. Dai and X. Chen, Photothermal therapy and photoacoustic imaging via nanotheranostics in fighting cancer, *Chem. Soc. Rev.*, 2019, **48**, 2053–2108.

109 X. Li, J. F. Lovell, J. Yoon and X. Chen, Clinical development and potential of photothermal and photodynamic therapies for cancer, *Nat. Rev. Clin. Oncol.*, 2020, **17**, 657–674.

110 Y. Xin, T. Liu and C. L. Yang, Development of PLGA-lipid nanoparticles with covalently conjugated indocyanine green as a versatile nanoplatform for tumor-targeted imaging and drug delivery, *Int. J. Nanomedicine*, 2016, **11**, 5807–5820.

111 Y. Zhang, X. Yue, B. Kim, S. Yao, M. V. Bondar and K. D. Belfield, Bovine serum albumin nanoparticles with fluorogenic near-IR-emitting squaraine dyes, *ACS Appl. Mater. Interfaces*, 2013, **5**, 8710–8717.

112 L. Huang, Z. Li, Y. Zhao, Y. Zhang, S. Wu, J. Zhao and G. Han, Ultralow-power near infrared lamp light operable targeted organic nanoparticle photodynamic therapy, *J. Am. Chem. Soc.*, 2016, **138**, 14586–14591.

113 T. M. Mohiuddin, C. Zhang, W. Sheng, M. Al-Rawe, F. Zeppernick, I. Meinhold-Heerlein and A. F. Hussain, Near infrared photoimmunotherapy: a review of recent progress and their target molecules for cancer therapy, *Int. J. Mol. Sci.*, 2023, **24**, 2655.

114 H. Kobayashi and P. L. Choyke, Near-infrared photoimmunotherapy of cancer, *Acc. Chem. Res.*, 2019, **52**, 2332–2339.

115 D. M. Cognetti, J. M. Johnson, J. M. Curry, S. T. Kochuparambil, D. McDonald, F. Mott, M. J. Fidler, K. Stenson, N. R. Vasan, M. A. Razaq, J. Campana, P. Ha, G. Mann, K. Ishida, M. Garcia-Guzman, M. Biel and A. M. Gillenwater, Phase 1/2a, open-label, multicenter study of RM-1929 photoimmunotherapy in patients with locoregional, recurrent head and neck squamous cell carcinoma, *Head Neck*, 2021, **43**, 3875–3887.

116 R. Okada, T. Kato, A. Furusawa, F. Inagaki, H. Wakiyama, D. Fujimura, S. Okuyama, H. Furumoto, H. Fukushima, P. L. Choyke and H. Kobayashi, Selection of antibody and light exposure regimens alters therapeutic effects of EGRF-targeted near-infrared photoimmunotherapy, *Cancer Immunol. Immunother.*, 2022, **71**, 1877–1887.

117 R. Okada, A. Furusawa, D. W. Vermeer, F. Inagaki, H. Wakiyama, T. Kato, T. Nagaya, P. L. Choyke, W. C. Spanos, C. T. Allen and H. Kobayashi, Near-infrared photoimmunotherapy targeting human-EGRF in a mouse tumor model simulating current and future clinical trials, *EBioMedicine*, 2021, **67**, 103345.

118 L. K. Bittner, S. A. Schonbichler, G. K. Bonn and C. W. Huck, Near infrared spectroscopy (NIRs) as a tool to analyze phenolic compounds in plants, *Curr. Anal. Chem.*, 2013, **9**, 417–423.

119 R. Kaavya, R. Pandiselvam, M. Mohammed, R. Dakshayani, A. Kothakota, S. V. Ramesh, D. Cozzolino and C. Ashokkumar, Application of infrared spectroscopy techniques for the assessment of quality and safety in spices: a review, *Appl. Spectrosc. Rev.*, 2020, **55**, 593–611.

120 D. Cozzolino, The sample, the spectra and the maths—the critical pillars in the development of robust and sound applications of vibrational spectroscopy, *Molecules*, 2020, **25**, 3674.

121 S. Balet, A. Guelpa, G. Fox and M. Manley, Rapid visco analyser (RVA) as a tool for measuring starch-related physiochemical properties in cereals: a review, *Food Anal. Methods*, 2019, **12**, 2344–2360.

122 N. Thanathornvarakul, J. Anuntagool and K. Tananuwong, Aging of low and high amylose rice at elevated temperature: mechanism and predictive modeling, *J. Cereal Sci.*, 2016, **70**, 155–163.

123 E. Izsó, M. Bartalné-Berceli, A. Salgó and S. Gergely, Monitoring of heat-treated wheat milling fractions by near infrared spectroscopic method, *Qual. Assur. Saf. Crop. Foods*, 2018, **10**, 93–102.

124 M. Schopf, M. C. Wehrli, T. Becker, M. Jekle and K. A. Scherf, Fundamental characterization of wheat gluten, *Eur. Food Res. Technol.*, 2021, **247**, 985–997.

125 R. Kaavya, R. Pandiselvam, M. Mohammed, R. Dakshayani, A. Kothakota, S. V. Ramesh, D. Cozzolino and C. Ashokkumar, Application of infrared spectroscopy techniques for the assessment of quality and safety in spices: a review, *Appl. Spectrosc. Rev.*, 2020, **55**, 593–611.

126 A. Khan, M. T. Munir, W. Yu and B. R. Young, Near-infrared spectroscopy and data analysis for predicting milk powder quality attributes, *Int. J. Dairy Technol.*, 2021, **74**, 235–245.

127 C. Wang, M. G. Reis, G. I. N. Waterhouse, Y. Hemar and M. M. Reis, Prediction of dairy powder functionality attributes using diffuse reflectance in the visible and near infrared (VIS-NIR) region, *Int. Dairy J.*, 2021, **117**, 104981.

128 L. Strani, S. Grassi, C. Alamprese, E. Casiraghi, R. Ghiglietti, F. Locci, N. Pricca and A. D. Juan, Effect of physicochemical factors and use of milk powder on milk rennet-coagulation: Process understanding by near infrared spectroscopy and chemometrics, *Food Control*, 2021, **119**, 107494.

129 D. Cozzolino, The ability of near infrared (NIR) spectroscopy to predict functional properties in foods: Challenges and opportunities, *Molecules*, 2021, **26**, 6981.

130 O. Y. Rodionova, L. P. Houmoller, A. L. Pomerantsev, P. Geladi, J. Burger, V. L. Dorofeyev and A. P. Arzamastsev, NIR spectrometry for counterfeit drug detection - A feasibility study, *Anal. Chim. Acta*, 2005, **549**, 151–158.
131 A. Paul, L. Wander, R. Becker, C. Goedecke and U. Braun, High-throughput NIR spectroscopic (NIRS) detection of microplastics in soil, *Environ. Sci. Pollut. Res.*, 2019, **26**, 7364–7374.
132 S. Sacher, J. Poms, J. Rehrl and J. G. Khinast, PAT implementation for advanced process control in solid dosage manufacturing-A practical guide, *Int. J. Pharm.*, 2021, **613**, 121408.